Interference Recycling: Effective Utilization of Interference for Enhancing Data Transmission

Zhao Li, *Member, IEEE*, Lijuan Zhang, Chengyu Liu, Siwei Le, Jie Chen, Kang G. Shin, *Life Fellow, IEEE*, Zheng Yan, *Fellow, IEEE*, and Jia Liu, *Senior Member, IEEE*

***Abstract*—With the rapid development of wireless communication technologies, Internet of Things (IoT) has emerged as one of the most important application scenarios. Due to the high density of IoT devices and the limited spectrum resources, along with the miniaturization and sustainability requirements of these devices, the development of low-cost interference management (IM) methods has become crucial for widespread use of IoT. Interference has long been known to harm network performance. Since a desired signal can be distorted by interference, and thus be incorrectly decoded at the destination, we argue that interference can also be transformed intentionally to extract the desired data from interfering signal(s). Based on this observation, we propose *Interference ReCycling* (IRC) for the IoT. Under IRC, a recycling signal is generated using the interference a victim IoT device is subjected to, and then sent by the device's associated gateway. Under the influence of the recycling signal, the desired data of the interfered/victim IoT transmission-pair can be recovered from the interference at the IoT device. We also show that the interfered user's spectral efficiency (SE) with IRC can be optimized further by properly distributing the transmit power used for the desired signal's transmission and the recycling signal. We validate the feasibility of IRC by implementing the method on the Universal Software Radio Peripheral (USRP) platform. Our theoretical analysis, experimental and numerical evaluation have shown that the proposed IRC can fully exploit interference, and hence can significantly improve the SE of the victim IoT device compared to other existing IM methods.**

***Index Terms*—IoT, interference management, signal processing, power allocation, spectral efficiency.**

I. Introduction

With the rapid development of wireless communication technologies and the advancement of integrated circuit techniques, people can communicate with each other via ubiquitous networks using continuously miniaturized electronic devices. Furthermore, these progressive technologies empower conventional equipment with intelligence, thereby enabling machine-type communications and facilitating the use of Internet of Things (IoT). According to forecasts, the number of IoT devices worldwide is expected to nearly double from 15.1 billion in 2020 to more than 29 billion in 2030 [1]. As a result, IoT is considered one of the most important application scenarios for 5G [2].

However, the widespread use of IoT still faces numerous challenges. First, the extremely high density of IoT devices (at least one million devices per square kilometer [3]) and the limited spectrum resources inevitably lead to inter-connection interferences, resulting in collisions among concurrent data transmissions sharing the same channel. Such interferences can impede IoT communications and disable critical IoT applications such as healthcare, manufacturing, and transportation. Second, due to the low-cost requirement and miniaturization of IoT devices, such as sensors and wearable devices, ensuring energy sustainability for wireless IoT devices becomes a significant challenge. Achieving secure and efficient data transmission, as well as simplified authentication, under strict constraints on power consumption and computational complexity is of practical significance for IoT.

To effectively address the aforementioned challenges, one approach is to develop low-cost interference management (IM) methods. Although there have been numerous IM methods, such as interference cancellation (IC) [4], interference alignment (IA) [5], [6], interference neutralization (IN) [7], interference steering (IS) [8], zero-forcing (ZF) reception, and zero-forcing beamforming (ZFBF), none of them are free of cost. Specifically, IC involves the reconstruction and subtraction of interference, which increases computational complexity and incurs the problem of error propagation [9]. IA consumes degrees-of-freedom (DoF) at the interfered receiver (Rx) and sacrifices the transmission performance of the interfering communication pairs. Both IN and IS consume transmit power for generating neutralizing and steering signals for IM. Additionally, similar to IA, IS also consumes DoF of the interfered Rx. As for ZF reception and ZFBF, they impair the reception performance of the desired signal and the interfering signals, respectively, while eliminating co-channel interference (CCI) among multiple concurrent data transmissions.

While researchers are making great efforts to suppress or mitigate interference as a negative factor, most of them neglect a crucial fact: in most practical cases, interferences are

Received 1 July 2024; revised 5 September 2024; accepted 20 September 2024. Date of publication 25 September 2024; date of current version 9 January 2025. This work was supported in part by the National Natural Science Foundation of China under Grant 62072351, Grant U23A20300, Grant 62202359, in part by the Key Research Project of Shaanxi Natural Science Foundation under Grant 2023-JC-ZD-35, in part by the 111 Center under Grant B16037, in part by JSPS KAKENHI under Grant JP23K16877, in part by the Project of Cyber Security Establishment with Inter-University Cooperation, and in part by the U.S. National Science Foundation under Grant 2245223. Recommended for acceptance by C. Xin. *(Corresponding author: Jia Liu.)*

Zhao Li, Lijuan Zhang, Chengyu Liu, Siwei Le, Jie Chen, and Zheng Yan are with the School of Cyber Engineering, Xidian University, Xi'an 710126, China (e-mail: zli@xidian.edu.cn; zyan@xidian.edu.cn).

Kang G. Shin is with the Department of Electrical Engineering and Computer Science, The University of Michigan, Ann Arbor, MI 48109 USA (e-mail: kgshin@umich.edu).

Jia Liu is with the Center for Strategic Cyber Resilience Research and Development, National Institute of Informatics, Chiyoda-ku 101-8430, Japan (e-mail: jliu@nii.ac.jp).

Digital Object Identifier 10.1109/TMC.2024.3467339

actually other unintended communication pairs' desired signals that carry both energy and data information. These signals can be leveraged to enhance the interfered communication. Although physical-layer network coding (PNC) [10] claims to utilize the known interference information in IM, its primary focus is still on the mitigation of interference. Another promising technique is energy harvesting (EH), which can convert energy from ambient radio frequency (RF) sources into electricity to autonomously power IoT devices [11]. However, since the energy conversion efficiency of RF signals is low [12], current EH technology can only produce small amounts of power, which is also highly dynamic and unpredictable. Therefore, the application of EH is limited.

To mitigate/overcome the above-mentioned deficiencies of existing IM methods, we propose a new concept called *interference recycling* (IRC) [13]. Based on IRC, both the energy and data information carried in the interference are leveraged to realize and enhance the interfered communication. By noting that interference to an unintended Rx is always a desired signal to its intended Rx, that is, the interfering signal also carries the data symbol; and moreover, a desired signal can be distorted by an interference, resulting in erroneous data decoding, we argue that the interference may also be affected likewise so that desired data is *erroneously recovered* from the interference. By exploiting the inter-plays among wireless signals, the victim Rx can recover its desired data from the combination of the interference and the recycling signal, thus achieving the goal of IRC. This paper makes three main contributions:

- Proposal of a novel data transmission scheme called *interference recycling* (IRC). By designing and using a recycling signal, the desired data is recovered from the interference and the victim Rx's spectral efficiency (SE) is improved significantly.
- Development of various IRC implementations. We show that the interfered user's SE with IRC can be optimized further by properly distributing the transmit power used for the desired signal's transmission and the recycling signal. We then present the optimal design of IRC (OIRC).
- Experimental validation of the proposed method using the USRP platform, alongside numerical evaluation.

The rest of this paper is organized as follows. Section II surveys related works, while Section III describes the system model. Section IV details the IRC and Section V presents various implementations and optimal design of IRC. Section VI validates the feasibility and evaluates the performance of IRC. Finally, Section VII concludes the paper.

Throughout this paper, we use the following notations. The set of complex numbers is denoted as $\mathbb{C}$, while vectors/matrices are represented by bold lower-case or upper-case letters. Let $\mathbf{X}^T$, $\mathbf{X}^H$ and $\mathbf{X}^{-1}$ be the transpose, Hermitian and inverse of matrix $\mathbf{X}$, respectively. $\|\cdot\|$ and $|\cdot|$ represent the Euclidean norm and the absolute value, respectively. $\mathbb{E}(\cdot)$ denotes statistical expectation and $\langle \mathbf{a}, \mathbf{b} \rangle$ represents the inner product of two vectors.

II. Related Works

Among typical IM methods, IC is performed by reconstructing the decoded signal component and removing it from the mixed received signal, so as to reduce the dimension of the signal to be processed at the next level and achieve the purpose of improving the data transmission rate of the system [4]. A typical application of IC is successive interference cancellation (SIC) [9], which is a multi-user detection (MUD) technology that utilizes the characteristics of signal structure to recover multi-channel concurrent data. SIC can be viewed as an iterative application of IC, where the number of iterations depends on the number of signal components in the mixed received signal. However, due to the inability of ensuring the correctness of decoding each signal component, errors in previously decoded signals can propagate and affect the subsequent decoding and signal reconstruction, leading to a phenomenon known as error propagation. IA is a powerful technique for controlling interference and has been under development in recent years. By preprocessing signals at the transmitter (Tx), multiple interfering signals are mapped into a certain signal subspace. Consequently, the overall interference space at the Rx is minimized, leaving the remaining subspace free from interference [5], [6]. While IA effectively adjusts the characteristics of the transmitted interferences at the interfering sources to achieve alignment at the victim Rx, this adjustment causes the signals no longer match their respective channels, leading to a degradation in the performance of interfering communication pairs. Additionally, at the interfered Rx, at least one DoF is required to accommodate the aligned interferences. This consumption of DoF can be considered a spatial resource cost for IA. The authors of [7] presented an interference neutralization (IN) scheme. A neutralizing signal with the same amplitude and opposite phase with respect to the interference is constructed and transmitted, so that the interference is cancelled at the interfered Rx, thereby achieving interference-free reception of the desired signal. However, the implementation of IN requires consuming additional transmit power to generate the neutralizing signal. By taking into account the power overhead of IN, dynamic interference neutralization (DIN) was proposed in [14]. DIN can balance the benefits brought by and power cost of IN by optimally distributing the transmit power used for the desired signal's transmission and the neutralizing signal. By recognizing that interference can not only be mitigated but also be modified, IS was proposed in [8]. IS employs a steering signal to adjust the interference perceived by the victim Rx to a direction orthogonal to the desired signal, thereby achieving interference-free transmission of the desired signal. However, similar to IN/DIN, IS also consumes transmit power, and like IA, it incurs a DoF cost. Based on the above discussion, all IM methods consume certain communication resources, which can potentially impair the performance of data transmission. Moreover, expensive IM methods would make it difficult to achieve energy sustainability of IoT devices. Therefore, finding ways to substantially utilize interference and develop low-cost IM methods is of practical significance.

As for the research on interference utilization, [10] proposed PNC for the first time. By utilizing the known interference information in data encoding, disturbance to unintended Rxs can be mitigated effectively. PNC suggests making use of interference instead of simply treating it as a nuisance [15]. Although PNC, similarly to IN/DIN and IS, attempts to make use of characteristics of and data information carried by interference, its focus is still on the elimination of interference energy. Nevertheless, substantial utilization of interference remains unaddressed. As

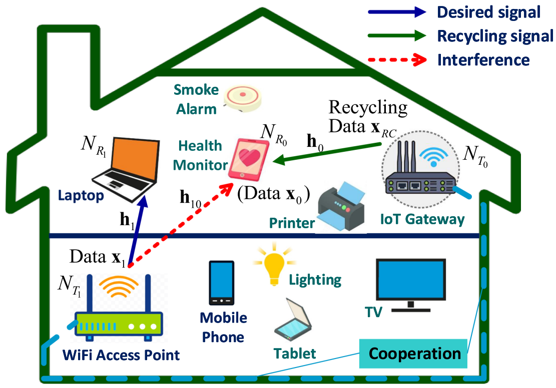

Fig. 1. System model.

a consequence, researchers have proposed wireless EH technology [16], [17], [18], [19] with which wireless nodes can harvest energy from their environment. However, while harvesting the interferences' energy, the desired signal is still subjected to disturbances. Additionally, this technique overlooks the potential utilization of data information carried by the interference. On the other hand, software-defined network (SDN) has emerged as a promising technology that offers centralized control, efficient resource management, and programmability, making it a significant enabler for the development of IoT [20], [21]. By leveraging SDN, the interfered IoT communication pair gains the capability to collaboratively interact with the interferer. This collaboration allows it to acquire the information about the interference's propagation characteristics and data content. Subsequently, the interfered communication pair can fully exploit this acquired information to achieve effective interference utilization and efficiently accomplish its desired data transmission.

III. System Model

We consider downlink transmission in a heterogeneous wireless network scenario where IoT coexists with a WiFi network, sharing the same spectrum [22], [23], [24]. As shown in Fig. 1, WiFi access point (AP) and IoT gateway (GW) [25] are equipped with N_{T_1} and N_{T_0} antennas, whereas the WiFi station (STA) and IoT device have N_{R_1} and N_{R_0} antennas, respectively. We use P_{T_1} and P_{T_0} to denote the transmit power of AP and GW. In this communication scenario, both the IoT and WiFi networks contain multiple subscribers. By employing a proper scheduling or resource allocation scheme, interior interference among multiple downlink data transmissions within a single network can be avoided. However, inter-network disturbance exists [26]. Without loss of generality, we assume that one WiFi data transmission (e.g., from AP to the laptop) coexists with an IoT transmission (e.g., from GW to the health monitor) at a time, and the AP's transmitted signal interferes with the IoT device, as depicted in Fig. 1. Since IoT devices have strict constraints on energy consumption and computational power, a low-cost IM method is crucial for IoT applications. In contrast, WiFi terminals possess relatively stronger processing capabilities and power supplies, allowing the WiFi network to employ existing IM methods as mentioned in Section II. Consequently, our focus lies on designing a low-cost and energy-efficient IM method specifically for IoT, with an emphasis on optimizing the transmission performance of IoT devices.

Let $\mathbf{h}_0 \in \mathbb{C}^{N_{R_0}\times N_{T_0}}$ and $\mathbf{h}_1 \in \mathbb{C}^{N_{R_1}\times N_{T_1}}$ be the channel matrices from GW to IoT device and from AP to STA, respectively, while channel state information (CSI) from AP to IoT device is denoted as $\mathbf{h}_{10} \in \mathbb{C}^{N_{R_0}\times N_{T_1}}$. We adopt a spatially uncorrelated Rayleigh flat fading channel model to model the elements of the above matrices as independent and identically distributed zero-mean unit-variance complex Gaussian random variables. We assume that all WiFi STAs and IoT devices experience block fading. Each terminal can accurately estimate CSI[1] with respect to its intended and unintended Txs and feed it back to the associated AP/GW via a low-rate error-free link. We assume reliable links for the delivery of CSI and signaling. The delivery delay is negligible relative to the time scale at which the channel state varies [28], [29], [30]. Let $\mathbf{x}_1$ and $\mathbf{x}_0$ denote the desired data vectors from AP and GW to their serving subscribers. $\mathbb{E}(\|\mathbf{x}_0\|^2) = \mathbb{E}(\|\mathbf{x}_1\|^2) = 1$ holds. For clarity of exposition, we assume the use of beamforming (BF), i.e., only one data stream is sent from AP to STA and from GW to IoT device, respectively. Then, $\mathbf{x}_1$ and $\mathbf{x}_0$ become scalars x_1 and x_0.[2] Since WiFi AP and IoT GW are deployed and managed by one owner, we assume that the GW can acquire the information of x_1 via collaboration with the AP.[3] Using this information, a recycling signal carrying data x_{RC} is generated by the GW and sent to its serving IoT device. Consequently, the desired data of the IoT device, i.e., x_0, can be recovered from the disturbance at the IoT device by utilizing the IRC signal. In this system model, it should be noted that the IoT device's desired data x_0 is not directly sent by the GW,[4] but is extracted from the interference. Moreover, besides utilizing the unlicensed ISM band as assumed in the current system model, IoT can also operate in other frequency bands, including cellular, Long-Term Evolution (LTE), and more. Consequently, when IoT coexists with these systems, it is susceptible to interference. Therefore, the system model proposed in this paper can be extended to other application scenarios as well.

[1]The inaccuracy of CSI does not cause the proposed method to be unusable, but leads to inaccurate generation of the recycling signal and interactions between the interference and the recycling signal, ultimately degrading the performance of the proposed method [27]. However, since our focus is on the utilization of interference, we will not explore the impact of imperfect CSI on the method's performance in this paper.

[2]The discussion of extending our method to more general application scenarios, where multiple data streams are sent from the AP and GW, can be found in our previous work [13]. For brevity, we avoid its repetition in this paper.

[3]In practice, a high-speed wired backhaul can be utilized to support information sharing between the GW and the AP. Moreover, since the backhaul is dedicated to signaling transmission and is separated from the data transmission channel, the cost of the information sharing will not affect the performance of our scheme.

[4]If the GW directly sends x_0, the IoT device will be interfered with by the signal sent from the WiFi AP, necessitating the use of other IM strategies to address this issue. As these conventional IM methods typically treat interference as harmful/hostile and aim to mitigate its influence on the desired transmission, they may exhibit lower transmission efficiency than our approach, which will be detailed in Section VI-B. Therefore, we begin our method design with the assumption of the GW directly sending x_0. However, our method can be extended to the scenario where the GW transmits both x_0 and x_{RC} simultaneously, as will be elaborated in Section V.

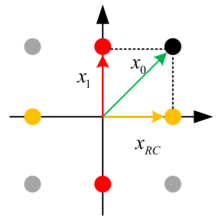

Fig. 2. Illustration of the basic principle of interference recyling.

IV. Design of Interference Recycling

For clarity of exposition, we assume that BF is adopted. However, the following discussion under a simplified parameter setting and use of BF for transmissions in IoT and WiFi networks can be extended to more general settings.

A. Theoretical Basis

The received signal at IoT device is expressed as

$$\mathbf{y}_0 = \sqrt{P_{T_1}}\mathbf{h}_{10}\mathbf{p}_1 x_1 + \sqrt{P_{T_0}}\mathbf{h}_0\mathbf{p}_{RC} x_{RC} + \mathbf{z}_0 \qquad (1)$$

where $\mathbf{p}_1$ represents the precoding vector for x_1 at WiFi AP; $\mathbf{p}_{RC}$ is the precoder for x_{RC} at IoT GW; and x_{RC} is the data symbol carried by the recycling signal. The first term on the right-hand side (RHS) of (1) denotes the interference from AP and the second term is the IRC signal sent from GW. $\mathbf{z}_0$ represents for the additive white Gaussian noise (AWGN) vector whose elements have zero-mean and variance σ_n^2. Note that in (1), GW sends an IRC signal instead of its desired signal.

IoT device employs a filter vector $\mathbf{f}_0$ to obtain the estimated signal $\bar{y}_0$ as

$$\bar{y}_0 = \mathbf{f}_0^H(\sqrt{P_{T_1}}\mathbf{h}_{10}\mathbf{p}_1 x_1 + \sqrt{P_{T_0}}\mathbf{h}_0\mathbf{p}_{RC} x_{RC}) + \mathbf{f}_0^H\mathbf{z}_0. \quad (2)$$

To recover the desired data, say x_0, at IoT device, the first term on the RHS of (2) should satisfy

$$\mathbf{f}_0^H(\sqrt{P_{T_1}}\mathbf{h}_{10}\mathbf{p}_1 x_1 + \sqrt{P_{T_0}}\mathbf{h}_0\mathbf{p}_{RC} x_{RC}) = \alpha x_0. \quad (3)$$

We define $\bar{x}_0 = \alpha x_0$ where α is a real number, i.e., the phase of $\bar{x}_0$ is either identical (α is positive) or opposite (α is negative) to that of x_0. From (3), the IRC signal can be determined, as elaborated in the next subsection.

Before delving into details, we first use Fig. 2 to illustrate the basic principle of IRC. It is well-known that data information can be represented by the amplitude and phase of a signal. In Fig. 2, we use two red dots to form a BPSK constellation with phase offsets of $\{\frac{\pi}{2}, \frac{3\pi}{2}\}$ (referred to as BPSK-I), while the two orange dots form a BPSK constellation with phase offsets of $\{0, \pi\}$ (referred to as BPSK-II). Similarly, the four gray/black dots form a QPSK constellation with phase offsets of $\{\frac{\pi}{4}, \frac{3\pi}{4}, \frac{5\pi}{4}, \frac{7\pi}{4}\}$. Without loss of generality, we assume that the red vector represents the BPSK-I modulated interference data x_1. To obtain the desired QPSK modulated data x_0 denoted by the green vector, a recycling data x_{RC} represented by the orange vector needs to be generated. This way, the recycling signal can interact with the interference at the interfered Rx to produce the desired signal.

B. Determination of the IRC Signal

According to (3), the maximum gain is achieved when the precoder and the receiving filter match the transmission channel. Let us consider pre- and post-processing based on the singular value decomposition (SVD) as an example, i.e., apply SVD to $\mathbf{h}_0$ to obtain $\mathbf{h}_0 = \mathbf{U}_0\mathbf{\Lambda}_0\mathbf{V}_0^H$ and adopt $\mathbf{p}_{RC} = \mathbf{v}_0^{(1)}$ and $\mathbf{f}_0 = \mathbf{u}_0^{(1)}$ at GW and IoT device, respectively, where $\mathbf{v}_0^{(1)}$ and $\mathbf{u}_0^{(1)}$ represent the first column vectors of the right and left singular matrices $\mathbf{V}_0$ and $\mathbf{U}_0$. Since an arbitrary symbol can be represented by its magnitude and phase, the desired, interfering, and recycling data symbols carried by their associated signals can be expressed as $x_0 = \rho_0 e^{j\theta_0}$, $x_1 = \rho_1 e^{j\theta_1}$, and $x_{RC} = \rho_{RC} e^{j\theta_{RC}}$. By defining $\beta = [\mathbf{u}_0^{(1)}]^H\mathbf{h}_{10}\mathbf{p}_1$ which is a complex number, we can rewrite (3) as

$$\sqrt{P_{T_1}}\beta\rho_1 e^{j\theta_1} + \sqrt{P_{T_0}}\lambda_0^{(1)}\rho_{RC} e^{j\theta_{RC}} = \alpha\rho_0 e^{j\theta_0}, \quad (4)$$

where $\lambda_0^{(1)}$ is the largest singular value of $\mathbf{h}_0$.

$$\begin{aligned}&\varepsilon\sqrt{P_{T_0}}[\mathrm{Re}(\beta) + j\mathrm{Im}(\beta)]\rho_1(\cos\theta_1 + j\sin\theta_1)\\&\quad + \sqrt{P_{T_0}}\lambda_0^{(1)}\rho_{RC}(\cos\theta_{RC} + j\sin\theta_{RC})\\&= \alpha\rho_0(\cos\theta_0 + j\sin\theta_0) \end{aligned} \quad (5)$$

In (4), α, ρ_{RC}, and θ_{RC} are variables of which ρ_{RC} and θ_{RC} determine the IRC signal. Using different values of ρ_{RC} and θ_{RC}, various signals satisfying (4) can be obtained to realize IRC, but the amplitude gains, i.e., $|\alpha|$, may vary. In order to maximize the desired signal's power (or amplitude gain) and make full use of transmit power P_{T_0} at GW, the optimal value of ρ_{RC} should be adopted so as to maximize $|\alpha|$. After obtaining the optimal ρ_{RC} and the corresponding α, we can compute θ_{RC} (see (13)) and thus construct the IRC signal.

For clarity of presentation, we define $\varepsilon = \sqrt{P_{T_1}}/\sqrt{P_{T_0}}$. By replacing the complex number in (4) with the sum of its real and imaginary parts, and expressing the complex exponentials in terms of Euler's formula, we can get (5) as below. Then, by writing equations based on the real and imaginary parts of (5), respectively, and defining two variables $A = \varepsilon\rho_1[\mathrm{Re}(\beta)\cos\theta_1 - \mathrm{Im}(\beta)\sin\theta_1]$ and $B = \varepsilon\rho_1[\mathrm{Re}(\beta)\sin\theta_1 + \mathrm{Im}(\beta)\cos\theta_1]$, we can have

$$\begin{cases}\lambda_0^{(1)}\rho_{RC}\cos\theta_{RC} = \frac{1}{\sqrt{P_{T_0}}}\alpha\rho_0\cos\theta_0 - A\\ \lambda_0^{(1)}\rho_{RC}\sin\theta_{RC} = \frac{1}{\sqrt{P_{T_0}}}\alpha\rho_0\sin\theta_0 - B\end{cases}. \quad (6)$$

$$\begin{aligned}&\cos^2\theta_{RC} + \sin^2\theta_{RC} = \left[\sqrt{P_{T_0}}\lambda_0^{(1)}\rho_{RC}\right]^{-2}\\&\quad\cdot\left[(\alpha\rho_0\cos\theta_0 - \sqrt{P_{T_0}}A)^2 + (\alpha\rho_0\sin\theta_0 - \sqrt{P_{T_0}}B)^2\right] = 1\end{aligned} \quad (7)$$

$$\begin{aligned}&(\alpha\rho_0\cos\theta_0 - \sqrt{P_{T_0}}A)^2 + (\alpha\rho_0\sin\theta_0 - \sqrt{P_{T_0}}B)^2\\&= \left[\sqrt{P_{T_0}}\lambda_0^{(1)}\rho_{RC}\right]^2\end{aligned} \quad (8)$$

$$\begin{aligned}&\alpha^2\rho_0^2 - 2\sqrt{P_{T_0}}\alpha\rho_0(A\cos\theta_0 + B\sin\theta_0)\\&\quad + P_{T_0}\left\{A^2 + B^2 - [\lambda_0^{(1)}]^2\rho_{RC}^2\right\} = 0\end{aligned} \quad (9)$$

In order to satisfy the power constraint of GW, $0 < \rho_{RC} \leq 1$ should hold.

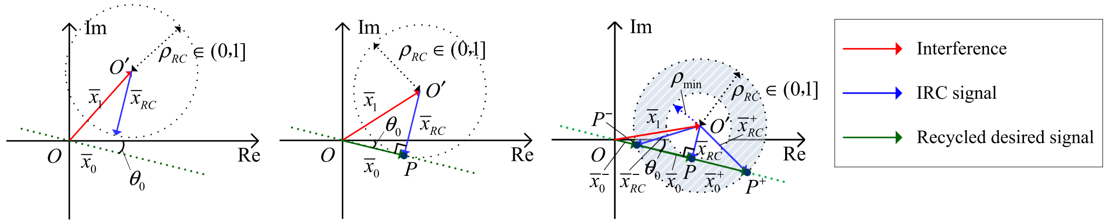

(a) No solution (b) Single solution (c) Double solution

Fig. 3. The principle of IRC and various relationships among interference, recycling signal, and recycled desired signal.

According to (4), when ρ_{RC} varies from 0 to 1, the relationship of the post-processed signals at the IoT device will be one of the following three situations as plotted in Fig. 3, where $\bar{x}_1 = \varepsilon\sqrt{P_{T_0}}\beta\rho_1 e^{j\theta_1}$, $\bar{x}_{RC} = \sqrt{P_{T_0}}\lambda_0^{(1)}\rho_{RC}e^{j\theta_{RC}}$, and $\bar{x}_0 = \alpha\rho_0 e^{j\theta_0}$. One should note that the amplitude of recycling signal is determined cooperatively by ρ_{RC} and $\sqrt{P_{T_0}}$. Since in the current design, we assume fixed $\sqrt{P_{T_0}}$, i.e., all transmit power of GW is used for generating the recycling signal, we only show the influence of ρ_{RC} on the solution(s) of α in Fig. 3. Our further study in Section V deals with the optimal amount of power that should be used for the IRC signal while the rest can be allocated to the direct desired signal's transmission.

Fig. 3 illustrates the principle of IRC and the relationships among interference, recycling signal, and recycled desired signal, where the green dotted line goes through the origin on which the desired data x_0 lies. In Fig. 3(a), there is no intersection between the circle and the green dashed line, and hence, given P_{T_0}, no IRC signal exists to extract desired data from interference. In Fig. 3(b), the green dotted line is tangent to the bottom of the circle when and only when $\rho_{RC} = 1$, and thus IRC signal with transmit power P_{T_0} can convert interference to the desired signal. As for Fig. 3(c), when $\rho_{RC} < \rho_{\min}$ where $\rho_{\min} < 1$, no IRC solution exists, while given $\rho_{RC} = \rho_{\min}$, only one solution for IRC signal exists. As ρ_{RC} varies from $\rho_{\min}$ to 1, there are two intersection points between the circle and the green dashed line, i.e., two IRC solutions, denoted by $\bar{x}_{RC}^{+}$ and $\bar{x}_{RC}^{-}$, exist to yield the recycled desired signal $\bar{x}_0^{+}$ and $\bar{x}_0^{-}$, respectively. Moreover, as can be seen from Fig. 3(c), $\bar{x}_0^{+}$, incurred by $\bar{x}_{RC}^{+}$, indicates a stronger desired signal power at the IoT device. In addition, in order to maximize the amplitude of $\bar{x}_0^{+}$, ρ_{RC} should be set to 1.

By applying the triangle formula to (6), we can get (7) below, which can be rewritten as (8).

Since the GW can acquire x_1 via collaboration with AP, A and B are known variables, so (8) can be regarded as a circle of the standard form $(x-a)^2 + (y-b)^2 = r^2$. The center and radius of the circle are $(a, b) = (\sqrt{P_{T_0}}A, \sqrt{P_{T_0}}B)$ and $r = \sqrt{P_{T_0}}\lambda_0^{(1)}\rho_{RC}$, respectively. By comparing (8) with Fig. 3, one can easily see that $(\sqrt{P_{T_0}}A, \sqrt{P_{T_0}}B)$ corresponds to O' and $r = |\bar{x}_{RC}|$. Moreover, the point represented by $(\alpha\rho_0\cos\theta_0, \alpha\rho_0\sin\theta_0)$ is not only on the circle with center O' as can be seen from (8), but also lies on the green dashed line indicating the desired data x_0, in that given an arbitrary point, say X, on the green dashed line, $\tan\theta_0 = \frac{\mathrm{Im}(X)}{\mathrm{Re}(X)}$ holds; likewise, the point $(\alpha\rho_0\cos\theta_0, \alpha\rho_0\sin\theta_0)$ on the circle satisfies $\tan\theta_0 = \frac{\alpha\rho_0\sin\theta_0}{\alpha\rho_0\cos\theta_0}$. θ_0 is the phase value of desired data x_0, and as shown in Fig. 3, it is the angle between the real axis and the green dashed line. So, $(\alpha\rho_0\cos\theta_0, \alpha\rho_0\sin\theta_0)$ represents P in Fig. 3(b), as well as P in Fig. 3(c) with $\rho_{RC} = \rho_{\min}$ and P^- and P^+ in Fig. 3(c) with $\rho_{RC} \in (\rho_{\min}, 1]$, respectively. On the other hand, (8) can be written as (9).

As can be seen from (8)–(9), ρ_{RC}^2 is a quadratic function of variable α. Since $\frac{\rho_0^2}{P_{T_0}[\lambda_0^{(1)}]^2} > 0$, ρ_{RC}^2 is a parabola opening upward, whose symmetry axis is

$$\alpha^* = \rho_0^{-1}\sqrt{P_{T_0}}(A\cos\theta_0 + B\sin\theta_0) \tag{10}$$

where α^* corresponds to the case when only one solution for α exists, i.e., $\alpha = \alpha^*$, as shown in Fig. 3(b) and (c) with $\rho_{RC} = \rho_{\min}$. Since $0 < \rho_{RC} \leq 1$, when $\alpha < \alpha^*$, both ρ_{RC}^2 and $\rho_{RC}^{+} = \sqrt{\rho_{RC}^2}$ decrease monotonically as α increases; otherwise, when $\alpha > \alpha^*$, ρ_{RC}^2 and ρ_{RC}^{+} grow as α increases. This is similar to the situation plotted in Fig. 3(c). As the figure shows, on the left side of point P, α decreases as ρ_{RC} increases, whereas on the right side of P, α increases as ρ_{RC} grows. Next, we will solve α from (9) under $\rho_{RC} = 1$, and then determine θ_{RC} based on (6), so that the IRC signal can be constructed.

By substituting $\rho_{RC} = 1$ into (9) and defining $D = \rho_0^2$, $E = -2\sqrt{P_{T_0}}\rho_0(A\cos\theta_0 + B\sin\theta_0)$ and $F = P_{T_0}(A^2 + B^2 - [\lambda_0^{(1)}]^2)$, (9) can be simplified to

$$D\alpha^2 + E\alpha + F = 0. \tag{11}$$

The solution to the above quadratic equation with one unknown can be obtained as

$$\alpha_{\pm} = (-E \pm \sqrt{E^2 - 4DF})/(2D). \tag{12}$$

Let $\Delta = E^2 - 4DF$, when $\Delta = 0$ and $\Delta > 0$, there will be one and two solutions for α, respectively. Otherwise, when $\Delta < 0$, no solution for α exists. When there are two solutions for α, we should adopt $\alpha = \begin{cases} \alpha_+, & |\alpha_+| \geq |\alpha_-| \\ \alpha_-, & |\alpha_+| < |\alpha_-| \end{cases}$ so as to maximize the magnitude of $\bar{x}_0$.

Based on the above discussion, we set $\rho_{RC} = 1$ to determine the parameters of recycling signal. If there is no solution for α, the transmit power of GW is not sufficient for IRC, needless to say $\rho_{RC} \in (0, 1)$. For this, we provide Corollary 1.

Corollary 1: If solution for α does not exist under $\rho_{RC} = 1$, given $\rho_{RC} < 1$, there is still no solution for α.

Sketch of proof: There are two ways to prove this Corollary. First, according to Fig. 3(a), if the circle with center O' and of radius $|\bar{x}_{RC}|$ does not intersect with the green dotted line on which the desired data x_0 is located under $\rho_{RC} = 1$, then the circle still cannot intersect with the desired data when $\rho_{RC} < 1$.

TABLE I
COMPARISON OF IRC AND OTHER IM METHODS

Feature \ Method	IRC	SIC	IA	IN/DIN	IS	PNC
Consumption of DoF	×	×	○	×	○	×
Iteration	×	○	×	×	×	×
Error propagation	×	○	×	×	×	×
Damage to the performance of interfering communication pair	×	×	○	×	×	×
Extra power cost	×	×	×	○	○	×
Utilization of interference data	○	×	×	×	×	○
Utilization of interference energy	○	×	×	×	×	×

Thus, Corollary 1 follows. Second, according to the power constraint of GW, non-existence of solutions for α means that even GW sets $\rho_{RC} = 1$, the recycling signal is still not strong enough for recovering the desired data from the interference. Therefore, when $\rho_{RC} < 1$, the amplitude of IRC signal decreases, so that α is still unavailable and hence IRC is not applicable. So, Corollary 1 follows. ∎

After obtaining α, we can calculate θ_{RC} following (13) (which is obtained by modifying (6)) as

$$\begin{cases} \cos\theta_{RC} = [\lambda_0^{(1)}\rho_{RC}]^{-1}\frac{1}{\sqrt{P_{T_0}}}\alpha\rho_0\cos\theta_0 - A \\ \sin\theta_{RC} = [\lambda_0^{(1)}\rho_{RC}]^{-1}\frac{1}{\sqrt{P_{T_0}}}\alpha\rho_0\sin\theta_0 - B \end{cases}. \tag{13}$$

The values of $\cos\theta_{RC}$ and $\sin\theta_{RC}$ are first calculated using (13). The range of θ_{RC} is then determined based on the values of both $\cos\theta_{RC}$ and $\sin\theta_{RC}$. Finally, the inverse trigonometric function is applied to obtain the value of θ_{RC}.

With $\rho_{RC} = 1$, α and θ_{RC}, an IRC signal can be constructed.

Based on the design of IRC, the IoT device needs the information of α to decode its desired data correctly. Otherwise, if α is unavailable at the IoT device and the desired data contains amplitude modulation, the IoT device will not be able to get correct desired data from $\bar{x}_0$. But, if the desired data only contains phase modulation, e.g., M-ary phase shift keying (MPSK), only the polarity of α is required at the IoT device for correct decoding. Specifically, if $\alpha > 0$, the desired data x_0 and the recycled desired signal $\bar{x}_0$ are in the same phase; otherwise, if $\alpha < 0$, x_0 and $\bar{x}_0$ are in the opposite phase. Therefore, with the polarity of α, x_0 can be recovered from $\bar{x}_0$. In such a case, less overhead than delivering the value of α will be incurred, thus facilitating the use of IRC.

Although we take the positive correlation of the spatial features of the interference and desired signal as an example in plotting Fig. 3, these two signals may be negatively correlated in practice, i.e., the angle between these signals is larger than $\pi/2$. In such a case, we can generate an IRC signal negatively correlated with the desired transmission, but positively correlated with the interference. Then, from the interaction of the IRC signal and interference, a signal of opposite phase with respect to the desired signal can be obtained. Consequently, the IoT device can decode the desired data by employing a negative α.

Table I highlights the primary differences between IRC and other typical IM schemes, where symbols ○ and × indicate having and not having the corresponding feature, respectively. The table demonstrates several advantages of IRC over other schemes. First, IRC does not consume any spatial DoF. In contrast, IA requires additional spatial DoFs and can degrade the performance of interfering communication pairs. Second, IRC avoids the inherent error propagation in SIC. Third, although IRC requires a Tx that consumes power for generating and transmitting the recycling signal, this power is ultimately superimposed with interference and utilized by the intended Rx. Notably, IRC effectively leverages both the data in, and the energy of, interference, thus exploiting interference.

So far, we have presented the design of IRC under a single interfered IoT device and a single interference configuration. When multiple IoT devices are experiencing interference from the AP, we recommend using a scheduling method to select the IoT device whose desired data shares similar characteristics as the interference. Our method can then be applied directly. When there are multiple interferences affecting the IoT device, we can leverage the interactions among multiple wireless signals to obtain an effective aggregated interference at the IoT device, as demonstrated in [8]. The GW can then design a recycling signal based on this effective interference, allowing our method to be directly applicable. Additionally, since our method achieves the desired data transmission by utilizing interference, the SE performance of the interfered IoT device varies with the interference level. Specifically, when the interference is weak, less interference can be utilized, resulting in low SE at the interfered device. However, in this scenario, the GW can have sufficient power to convert the interference to the desired signal. This implies that our method has a high feasible probability. On the other hand, when the interference is strong, more interference can be leveraged for the desired transmission if the interference and the desired signal are positively correlated. However, if the correlation between the interference and the desired signal turns negative, the GW may not have enough power to recycle the strong interference. In such a case, the GW can design a recycling signal that aligns with the interference, resulting in a recycled signal with a phase opposite to the desired one. Consequently, the IoT device can retrieve the desired data by reversing the observed signal.

In scenarios with multiple APs, interference between them may occur. However, in practice, since the number of APs is much smaller than the number of STAs, the multiple interfering APs can use different frequency channels to avoid interference [31]. Consequently, the GW only needs to utilize the co-channel interference with our method. Moreover, recent advancements in IEEE 802.11be and IEEE 802.11ay include the Multiple-Access Point Coordination (MAP-Co) mechanism, which allows multiple APs to transmit data without interference or collisions [32]. Additionally, even if the AP needs to compete

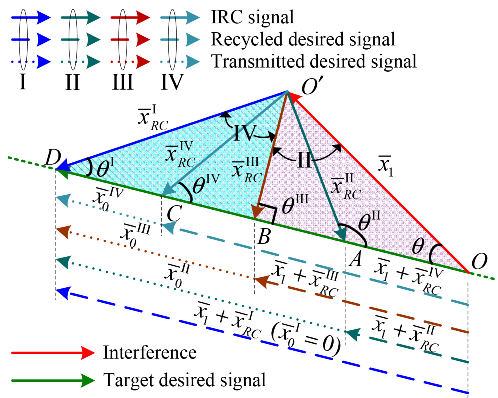

Fig. 4. Various designs of IRC.

for channel access similarly to the STAs, resulting in intermittent signal transmission, the GW can still utilize this intermittent interference with our method. First, the use of a high-speed backhaul ensures that interference information from the AP can be shared with the GW in real time, enabling the GW to generate a recycling signal to interact with the interference at IoT device. Second, the preamble (used for synchronization) length of a WiFi data packet is only 16 to 20 microseconds [33], while the channel, once acquired by an AP, can be occupied for up to 8.16 milliseconds [32], which is hundreds of times longer than the preamble. Therefore, the GW can synchronize with the interference within a short period of time and leverage it using our method. In practical applications, the interfered communication pair can selectively utilize the interference with a longer duration.

V. Various and Optimal Designs of IRC

In the previous section, we presented the design of IRC under the assumption that the GW consumes all of its power for recycling signal transmission. However, in practice, the GW can also send the desired data directly to the IoT device. In what follows, we will first present various designs of IRC, and then discuss the determination of an optimal power allocation factor at GW so as to maximize the achievable SE of IoT device. We refer to the IRC scheme that can optimally utilize the transmit power of GW for interference recycling and desired data transmission as *optimal interference recycling* (OIRC).

A. Various Designs of IRC

We will show various IRC realizations based on different transmit power allocation at the GW for the transmission of recycling and desired signals. Fig. 4 illustrates four IRC designs. Similarly to Fig. 3, the post-processed interference $\bar{x}_1$ is denoted by vector $\overrightarrow{OO'}$, while the recycled desired signal at the IoT device, $\bar{x}_0$, is represented by a green vector $\overrightarrow{OD}$. The angle between $\overrightarrow{OO'}$ and $\overrightarrow{OD}$ is denoted by θ. As the figure shows, with mode I, the GW allocates all the transmit power P_{T_0} to the IRC signal $\bar{x}^I_{RC}$ ($\overrightarrow{O'D}$) so as to obtain the recycled desired signal $\bar{x}_0$ ($\overrightarrow{OD}$) from the interference $\bar{x}_1$ ($\overrightarrow{OO'}$). In such a case, no power is allocated to the direct transmission of desired signal, denoted by $\bar{x}^I_0$, and hence $\bar{x}^I_0 = 0$. For a fair comparison, we let the other three IRC designs, indexed by II, III, and IV, respectively, yield an identical target desired signal $\overrightarrow{OD}$. We also define the angle θ^I which is the function of $\bar{x}_1$, $\bar{x}_0$, and P_{T_0}, and is thus expressed as $\theta^I = f(\bar{x}_1, \bar{x}_0, P_{T_0})$.

TABLE II
Comparison of Various IRC Designs

Mode index	$\theta^{\mathcal{M}}$	Tx power consumption
I	$\theta^I = f(\bar{x}_1, \bar{x}_0, P_{T_0})$	$= P_{T_0}$
II	$\theta^{II} \in (\frac{\pi}{2}, \pi - \theta)$	$> P_{T_0}$
III	$\theta^{III} = \frac{\pi}{2}$	$= P_{T_0}$
IV	$\theta^{IV} \in (\theta^I, \frac{\pi}{2})$	$< P_{T_0}$

As for mode II, the powers of post-processed IRC signal $\bar{x}^{II}_{RC}$ ($\overrightarrow{O'A}$) and desired signal $\bar{x}^{II}_0$ ($\overrightarrow{AD}$) are $|\bar{x}^{II}_{RC}|^2$ and $|\bar{x}^{II}_0|^2$, respectively. Hence, the total power consumption is $(|\bar{x}^{II}_{RC}|^2 + |\bar{x}^{II}_0|^2)/[\lambda^{(1)}_0]^2$. Let $\overrightarrow{OA}$ denote the recycled desired signal. The amplitude of the combination of the recycled and directly transmitted desired signal components is then $|\overrightarrow{OA} + \overrightarrow{AD}| = |\overrightarrow{OD}|$. In mode II, the interference is underutilized. Since $\cos(\pi - \theta^{II}) > 0$, we have $|\bar{x}^{II}_{RC}|^2 + |\bar{x}^{II}_0|^2 > |\bar{x}^I_{RC}|^2$. Therefore, the total transmit power of mode II is greater than that of scheme I, P_{T_0}; that is, mode II is inferior to mode I in power efficiency [34]. As the triangular shadow area determined by $\overrightarrow{OO'}$, $\overrightarrow{OB}$, and $\overrightarrow{O'B}$ shows, where angle $\theta^{II} \in (\frac{\pi}{2}, \pi - \theta)$, the design of mode II falls in this region.

In mode III, the filtered IRC signal $\bar{x}^{III}_{RC}$ ($\overrightarrow{O'B}$) and the desired signal $\bar{x}^{III}_0$ ($\overrightarrow{BD}$), with power $|\bar{x}^{III}_{RC}|^2$ and $|\bar{x}^{III}_0|^2$, respectively, are obtained by the IoT device simultaneously. $\theta^{III} = \frac{\pi}{2}$, and hence mode III makes full use of the interference. The combined desired signal at IoT device is $(\bar{x}_1 + \bar{x}^{III}_{RC}) + \bar{x}^{III}_0 = \overrightarrow{OB} + \overrightarrow{BD} = \overrightarrow{OD}$. According to the Pythagorean Theorem, $|\bar{x}^{III}_{RC}|^2 + |\bar{x}^{III}_0|^2 = |\bar{x}^I_{RC}|^2$ holds. So, mode III and I yield the same magnitude of desired signal ($|\overrightarrow{OD}|$) with an identical power consumption, i.e., P_{T_0}.

In mode IV, the filtered IRC signal $\bar{x}^{IV}_{RC}$ ($\overrightarrow{O'C}$) and the desired signal $\bar{x}^{IV}_0$ ($\overrightarrow{CD}$) have power $|\bar{x}^{IV}_{RC}|^2$ and $|\bar{x}^{IV}_0|^2$, respectively. The combined desired signal at the IoT device is $(\bar{x}_1 + \bar{x}^{IV}_{RC}) + \bar{x}^{IV}_0 = \overrightarrow{OD}$. Edges $\overrightarrow{O'B}$, $\overrightarrow{O'D}$, and $\overrightarrow{BD}$ enclose the region of mode IV where $\theta^{IV} \in (\theta^I, \frac{\pi}{2})$. Then, since $\cos(\pi - \theta^{IV}) < 0$, the inequality $|\bar{x}^{IV}_{RC}|^2 + |\bar{x}^{IV}_0|^2 < |\bar{x}^I_{RC}|^2$ holds. Therefore, to obtain the same magnitude of desired signal at the IoT device ($|\overrightarrow{OD}|$), mode IV consumes less power than I.

Table II compares different IRC designs under the constraint that the amplitude of the desired signal composed of the recycled and the directly transmitted parts (for mode I, however, the directly transmitted part is 0) should be the same. $\theta^{\mathcal{M}}$, where $\mathcal{M} \in \{I, II, III, IV\}$, represents the angle between the filtered IRC signal and the recycled desired signal with IRC mode $\mathcal{M}$. As one can infer from the table, given the same transmit power budget, mode IV is advantageous over the others in SE, while mode I and III rank the second, mode II yields the lowest SE. Moreover, by allocating the optimal amount of power, the performance of IRC mode IV can be optimized further.

B. Optimal Design of IRC

As discussed in the previous subsection, there exists an optimal power allocation strategy, yielding the maximum SE of the IoT device. In what follows, we will first illustrate the influence of the power allocation factor at the GW, denoted by μ, on the reception of IoT device, and then in the next subsection, elaborate on the verification of the existence and calculation of the optimal value of μ.

Recall that the transmit power of AP and GW are P_{T_1} and P_{T_0}. We let GW allocate $(1-\mu)P_{T_0}$ and μP_{T_0} to the desired data transmission and the IRC signal, respectively, where $\mu \in [0,1]$ represents the power allocation coefficient. Then, the received signal at IoT device can be written as

$$\mathbf{y}_0 = \sqrt{P_{T_1}}\mathbf{h}_{10}\mathbf{p}_1 x_1 + \sqrt{\mu P_{T_0}}\mathbf{h}_0\mathbf{p}_{RC}x_{RC} + \sqrt{(1-\mu)P_{T_0}}\mathbf{h}_0\mathbf{p}_0\kappa x_0 + \mathbf{z}_0 \tag{14}$$

where the first term on the RHS of (14) denotes the interference from AP. The second and third terms are the IRC signal and the desired signal sent from GW, respectively. x_0 is the data symbol carried by the desired signal, and $\mathbf{p}_0$ is the precoding vector employed for preprocessing x_0. The real number $\kappa \in \{-1, 1\}$ determines the additional phase offset of the desired signal. When $\kappa = 1$, the additional phase offset of the desired signal is 0, i.e., the GW directly precodes and sends the desired data x_0. When $\kappa = -1$, an additional phase of π is imposed on the desired signal. In this case, the GW first inverts data x_0, and then precodes it with $\mathbf{p}_0$ for the following transmission.

Similarly to (2), the IoT device employs filter $\mathbf{f}_0$ to obtain

$$\bar{y}_0 = \mathbf{f}_0^H\left(\sqrt{P_{T_1}}\mathbf{h}_{10}\mathbf{p}_1 x_1 + \sqrt{\mu P_{T_0}}\mathbf{h}_0\mathbf{p}_{RC}x_{RC}\right) + \sqrt{(1-\mu)P_{T_0}}\mathbf{f}_0^H\mathbf{h}_0\mathbf{p}_0\kappa x_0 + \mathbf{f}_0^H\mathbf{z}_0. \tag{15}$$

In order to recover the desired signal from interference, the first term on the RHS of (15) should satisfy (3). We take SVD-based pre-processing and filtering as an example, i.e., adopting $\mathbf{p}_0 = \mathbf{v}_0^{(1)}$ where $\mathbf{v}_0^{(1)}$ is the first column vector of the right singular matrix $\mathbf{V}_0$ resulting from $\mathbf{h}_0 = \mathbf{U}_0\mathbf{\Lambda}_0\mathbf{V}_0^H$. The values of $\mathbf{p}_{RC}$ and $\mathbf{f}_0$ are the same as those employed in (4). Then, based on the design in Section IV-B, we can have

$$\bar{y}_0 = \left[\alpha + \sqrt{(1-\mu)P_{T_0}}\lambda_0^{(1)}\kappa\right]x_0 + [\mathbf{u}_0^{(1)}]^H\mathbf{z}_0. \tag{16}$$

The first term on the RHS of the above equation represents the combined information [35] intended for IoT device. Note that $\sqrt{(1-\mu)P_{T_0}}\lambda_0^{(1)}$ is a positive real number, when α and κ are of the same sign, $\sqrt{(1-\mu)P_{T_0}}\lambda_0^{(1)}\kappa x_0$ obtained by filtering the desired signal directly sent from the GW, and the component $\bar{x}_0 = \alpha x_0$ recycled from the interference, will be a constructive combination. Otherwise, when α and κ are opposite in sign, $\sqrt{(1-\mu)P_{T_0}}\lambda_0^{(1)}\kappa x_0$ and αx_0 will be a destructive combination. Therefore, in order to achieve as high an amplitude gain of the desired data as possible, we should let α and κ have the same sign, i.e., we set $\kappa = 1$ for a positive α, whereas for a negative α, we employ $\kappa = -1$. That is, by introducing the additional phase offset coefficient κ, the recycled desired signal can be guaranteed to be constructive with the desired signal directly sent from the GW.

Next, we will discuss the computation of α. Recall that we have previously defined the complex variable $\beta = [\mathbf{u}_0^{(1)}]^H\mathbf{h}_{10}\mathbf{p}_1$ and the real number coefficient $\varepsilon = \sqrt{P_{T_1}}/\sqrt{P_{T_0}}$, the first term on the RHS of (15) satisfying (3) can be rewritten as

$$\varepsilon\sqrt{P_{T_0}}\beta x_1 + \sqrt{\mu P_{T_0}}\lambda_0^{(1)}x_{RC} = \alpha x_0. \tag{17}$$

Similarly to the derivation of (4) and (5), we substitute $x_1 = \rho_1 e^{j\theta_1}$, $x_0 = \rho_0 e^{j\theta_0}$, and $x_{RC} = \rho_{RC}e^{j\theta_{RC}}$ into (17) to obtain (18) and (19) below

$$\varepsilon\sqrt{P_{T_0}}[\mathrm{Re}(\beta) + j\mathrm{Im}(\beta)]\rho_1(\cos\theta_1 + j\sin\theta_1) + \sqrt{\mu P_{T_0}}\lambda_0^{(1)} \rho_{RC}(\cos\theta_{RC} + j\sin\theta_{RC}) = \alpha\rho_0(\cos\theta_0 + j\sin\theta_0) \tag{18}$$

$$\begin{cases} \sqrt{\mu}\lambda_0^{(1)}\rho_{RC}\cos\theta_{RC} = \frac{1}{\sqrt{P_{T_0}}}\alpha\rho_0\cos\theta_0 - A \\ \sqrt{\mu}\lambda_0^{(1)}\rho_{RC}\sin\theta_{RC} = \frac{1}{\sqrt{P_{T_0}}}\alpha\rho_0\sin\theta_0 - B \end{cases} \tag{19}$$

where $A = \varepsilon\rho_1[\mathrm{Re}(\beta)\mathrm{cos}\theta_1 - \mathrm{Im}(\beta)\mathrm{sin}\theta_1]$ and $B = \varepsilon\rho_1 [\mathrm{Re}(\beta)\mathrm{sin}\theta_1 + \mathrm{Im}(\beta)\mathrm{cos}\theta_1]$.

Then, by applying the triangle formula to (19), we can obtain (20) below. From (20) we can have:

$$\alpha^2\rho_0^2 - 2\sqrt{P_{T_0}}\alpha\rho_0(A\cos\theta_0 + B\sin\theta_0) + P_{T_0}\left\{A^2 + B^2 - \mu[\lambda_0^{(1)}]^2\rho_{RC}^2\right\} = 0 \tag{20}$$

$$D\alpha^2 + E\alpha + F_\mu = 0 \tag{21}$$

where $D = \rho_0^2$, $E = -2\sqrt{P_{T_0}}\rho_0(A\cos\theta_0 + B\sin\theta_0)$, and $F_\mu = P_{T_0}(A^2 + B^2 - \mu[\lambda_0^{(1)}]^2)$. Similarly to the discussion about (11), we let $\Delta_\mu = E^2 - 4DF_\mu$. When $\Delta_\mu = 0$ and $\Delta_\mu > 0$, there will be one and two solutions for α, respectively. Otherwise, when $\Delta_\mu < 0$, no solution for α exists. Given $\Delta_\mu \geq 0$, the solution for α is

$$\alpha_\pm = (-E \pm \sqrt{E^2 - 4DF_\mu})/(2D). \tag{22}$$

When there are two solutions for α, we should choose $\alpha = \begin{cases}\alpha_+, & |\alpha_+| \geq |\alpha_-| \\ \alpha_-, & |\alpha_+| < |\alpha_-|\end{cases}$ so as to maximize the magnitude of $\bar{x}_0 = \alpha x_0$. Accordingly, the calculation of the instantaneous SE of the IoT transmission-pair with IRC adopting parameter μ (denoted by $\mathcal{C}_0^{\mu IRC}$) can be formulated as the following optimization problem:

$$\mathcal{C}_0^{\mu IRC} = \max_{\mu\in[0,1]} \log_2\left\{1 + \frac{|x_0|^2}{\sigma_n^2}\left[\alpha + \sqrt{(1-\mu)P_{T_0}}\lambda_0^{(1)}\kappa\right]^2\right\}. \tag{23}$$

As (23) shows, maximizing $\mathcal{C}_0^{\mu\mathrm{IRC}}$ is equivalent to maximizing $|\alpha + \sqrt{(1-\mu)P_{T_0}}\lambda_0^{(1)}\kappa|$. By adopting an optimal μ^* where $\mu^* \in [0,1]$, $\mathcal{C}_0^{\mu IRC}$ can be maximized.

C. Calculation of μ^*

We now detail the calculation of the optimal μ^*. Based on (23), a μ that maximizes $[\alpha + \sqrt{(1-\mu)P_{T_0}}\lambda_0^{(1)}\kappa]^2$ can also yield the largest $\mathcal{C}_0^{\mu IRC}$ under the transmit power constraint at GW. Therefore, we define a variable $\gamma = |\alpha + \sqrt{(1-\mu)P_{T_0}}\lambda_0^{(1)}\kappa|$ and discuss the computation of μ^* so as to maximize γ.

As mentioned above, when μIRC (IRC adopting μ) is feasible, there is solution(s) for α, we rewrite (22) and obtain (24). By defining $Q = \frac{\sqrt{P_{T_0}}(A\mathrm{cos}\theta_0 + B\mathrm{sin}\theta_0)}{\rho_0}$, $R = [\frac{\lambda_0^{(1)}\rho_{RC}\sqrt{P_{T_0}}}{\rho_0}]^2$, and

$S = \frac{P_{T_0}(A\sin\theta_0 - B\cos\theta_0)^2}{\rho_0^2}$, (24) can be simplified to

$$\alpha_{\pm} = \frac{\sqrt{P_{T_0}}(A\cos\theta_0 + B\sin\theta_0)}{\rho_0} \pm \sqrt{\left[\frac{\lambda_0^{(1)}\rho_{RC}\sqrt{P_{T_0}}}{\rho_0}\right]^2 \mu - \frac{P_{T_0}(A\sin\theta_0 - B\cos\theta_0)^2}{\rho_0^2}} \tag{24}$$

$$\alpha_{\pm} = Q \pm \sqrt{R\mu - S}. \tag{25}$$

Then, the solution for α becomes (26).

$$\alpha = \begin{cases} \alpha_{+} = Q + \sqrt{R\mu - S}, & |Q + \sqrt{R\mu - S}| \geq |Q - \sqrt{R\mu - S}| \\ \alpha_{-} = Q - \sqrt{R\mu - S}, & |Q + \sqrt{R\mu - S}| < |Q - \sqrt{R\mu - S}| \end{cases} \tag{26}$$

When α is positive, we set $\kappa = 1$. In this case, if $Q \geq 0$ we can have $\alpha = \alpha_{+} = Q + \sqrt{R\mu - S}$; otherwise, if $Q < 0$, we get $\alpha = \alpha_{-} = Q - \sqrt{R\mu - S} < 0$, but this contradicts $\alpha > 0$. Therefore, α should be taken as $\alpha_{+} = Q + \sqrt{R\mu - S}$. By defining $K = \sqrt{P_{T_0}}\lambda_0^{(1)}$ and substituting the expression of α into γ, we have

$$\gamma = K\sqrt{1-\mu} + Q + \sqrt{R\mu - S}. \tag{27}$$

By computing the derivative of γ with respect to μ and setting it to 0, we get

$$\frac{\partial\gamma}{\partial\mu} = -\frac{K}{2\sqrt{1-\mu}} + \frac{R}{2\sqrt{R\mu - S}} = 0. \tag{28}$$

Then, the extreme value of γ can be achieved when

$$\mu = \mu^* = (R^2 + SK^2)/(K^2R + R^2). \tag{29}$$

When α is negative, we set $\kappa = -1$. In this case, if $Q < 0$, we adopt $\alpha = \alpha_{-} = Q - \sqrt{R\mu - S}$; otherwise, if $Q \geq 0$, we can get $\alpha = \alpha_{+} = Q + \sqrt{R\mu - S} > 0$, which contradicts $\alpha < 0$. Therefore, α should be taken as $\alpha_{-} = Q - \sqrt{R\mu - S}$. By substituting α into γ, we have

$$\gamma = K\sqrt{1-\mu} - Q + \sqrt{R\mu - S}. \tag{30}$$

Similarly to the previous analysis of (27)–(29), by computing the derivative of γ with respect to μ and setting it to 0, we get the extreme point of γ when $\mu = \mu^*$ is taken according to (30).

From the above analysis we can conclude that regardless whether α is positive or negative, μ^* given by (29) can yield the extreme value of γ.

Then, we prove μ^* can yield the maximum γ. We rewrite (28) as

$$\frac{\partial\gamma}{\partial\mu} = \frac{R\sqrt{1-\mu} - K\sqrt{R\mu - S}}{2\sqrt{(1-\mu)(R\mu - S)}}. \tag{31}$$

Since $2\sqrt{(1-\mu)(R\mu - S)} > 0$, $R > 0$, $K > 0$, $\mu \in [0,1]$, and $R\sqrt{1-\mu^*} - K\sqrt{R\mu^* - S} = 0$, we can easily see that when $\mu < \mu^*$, the inequality $R\sqrt{1-\mu} - K\sqrt{R\mu - S} > 0$ holds. Therefore, we have $\frac{\partial\gamma}{\partial\mu} > 0$ given $\mu < \mu^*$. Similarly, when $\mu > \mu^*$, we can get $R\sqrt{1-\mu} - K\sqrt{R\mu - S} < 0$, and hence $\frac{\partial\gamma}{\partial\mu} < 0$ provided $\mu > \mu^*$. Then, μ^* yields the maximum γ. Recall that $\mu \in [0,1]$, we then verify μ^* lies in the region of [0,1], i.e., μ^* can be used for the allocation of transmit power at the GW so as to realize interference recycling. As can be seen from (22) and (25), when $\Delta_\mu = 0$, i.e., $R\mu - S = 0$, there exists only one solution for α. In such a case, we get $\mu = S/R$.

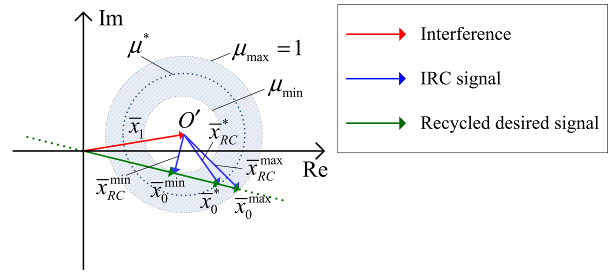

Fig. 5. An illustration of the impact of μ on the realization of μIRC.

Fig. 5 plots the impact of μ on the design of μIRC. We employ $\rho_{RC} = 1$ based on the discussion in Section IV-B, and hence, given P_{T_0}, the amplitude of the recycling signal is determined by μ. Therefore, we only show the influence of μ on the feasibility of μIRC in Fig. 5. As shown in the figure, there is only one intersection point between the IRC signal and the green dashed line where the desired data x_0 lies, under $\mu = S/R$, and no intersection point exists in the case of $\mu < S/R$. Since S/R is the minimum power allocation coefficient for realizing interference recycling, we define $\mu_{\min} = S/R$. When $\mu = \mu_{\min}$, $\bar{x}_0^{\min}$ is recycled from the mixed signal consisting of IRC signal $\bar{x}_{RC}^{\min}$ and the interference $\bar{x}_1$. Otherwise, given $\mu < \mu_{\min}$, $\Delta_\mu = R\mu - S < 0$ holds, no solution for (21) exists, and hence interference recycling is not applicable. Since $\mu_{\min} \in [0,1]$, $R \geq S$ should be satisfied. Otherwise, transmit power of GW will be insufficient for implementing IRC. Substituting $R \geq S$ into (29), we have $\mu^* = \frac{R^2 + SK^2}{K^2R + R^2} \leq 1$. That is, when $\mu_{\min} \in [0,1]$, we can obtain $\mu^* \in [\mu_{\min}, 1]$. In Fig. 5, we define $\mu_{\max} = 1$.

Based on the above discussion, the optimal power allocation for μIRC, called *optimal interference recycling* (OIRC), can be realized. It should be noted that when $R < S$, $\mu_{\min} > 1$ can be derived from $\Delta_\mu = 0$, and in such a case, the GW does not have enough power to realize IRC.

When OIRC is applied for data transmission where both phase and amplitude modulation are involved, the GW needs to send α and μ to the IoT device for data recovery. Since both α and μ are related to certain transmit symbol and channel conditions, computing and transmitting α and μ will incur too large overhead to employ OIRC. However, given a modulation scheme, the number of possible symbol waveforms is fixed. So, in a channel block where the channel parameters, interference status, and inter-relation of the desired and interfering signals remain constant, α and μ for each of the combinations of the above-mentioned factors are calculated only once. That is, if the channel varies slowly or/and the modulation order is not too high, the computational complexity could be acceptable. Specifically, in the beginning of a block, the Tx computes all possible combinations of α and μ based on the underlying modulation scheme and CSI within the block. Thus-computed αs and μs are then delivered to the Rx. During the subsequent data transmission, Tx only needs to send an index indicating which α and μ should be used in decoding the desired data along with the IRC signal to Rx which can then recycle the desired data with such information. If an index which is the same as the previous received one(s) by the Rx, the data associated with such same previous index can be outputted directly without performing the

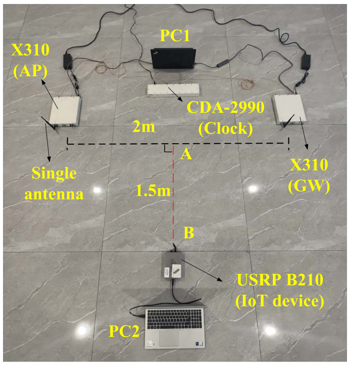

Fig. 6. Hardware implementation of IRC.

recycling process in Section V-B. However, when only phase modulation is employed, i.e., no amplitude modulation is involved; only the complexity related to α is required for realizing OIRC. In summary, the main computational complexity lies in the beginning of a block, while significantly simplifying the processing for the subsequent transmission of the same block. The detailed analysis of OIRC's complexity and its design with less complexity/cost are part of our future inquiry.

It should be noted that the signal transmission from the GW to IoT device can cause interference to the STA. However, since the transmit power of the GW is fixed at P_{T_0}, our methods will not introduce additional interference to the WiFi STA as compared to the conventional communication scheme. Specifically, in a conventional scheme, the entire power P_{T_0} is dedicated to transmitting the desired signal from the GW to the IoT device. In contrast, with IRC, all of P_{T_0} is used to generate the recycling signal, resulting in identical interference power at the STA as compared to the conventional scheme. With OIRC, a portion of P_{T_0} is allocated to generate the recycling signal, while the remainder is used for direct transmission of the desired signal. Since the total transmit power of the recycling and desired signals is P_{T_0} , the power of the combined interference at the STA will be statistically identical to that with the conventional scheme.

VI. Evaluation

In this section, we first corroborate IRC via its implementation on USRP devices and then evaluate its performance via MATLAB simulation. Without loss of generality, we take BPSK modulation at Txs and QPSK demodulation at Rx as an example to illustrate the implementation of IRC. Similar results can be obtained with other modulation schemes.

A. Hardware Implementation

We utilize two USRP X310 devices each equipped with a UBX-160 radio frequency (RF) daughterboard, along with a USRP B210 device to implement the IRC. This setup can demonstrate the IRC capability for accurate data transmission and effective interference management. As illustrated in Fig. 6, the two USRP X310 devices serve as the interfering Tx (i.e., AP) and the interfered Tx (i.e., GW) in IRC, respectively. They are connected to a CDA-2990 which generates a high-accuracy 1 pulse per second (PPS) and 10MHz reference signal for device synchronization. The USRP B210 device acts as the legitimate Rx (IoT device). Since we focus on the IM at the interfered Rx, we omit the implementation of STA in our experimental setup. All devices are located on the same horizontal plane, and the two Txs are separated by 2 m. The X310 devices are connected to a computer, denoted as PC1, which controls the data modulation and signal transmission at AP and GW.[5] Similarly, the B210 device is connected to another computer, denoted as PC2, which controls signal reception and data demodulation of IoT device. For simplicity, we deploy the desired Rx (point B) on the mid-perpendicular line between the two Txs, with both Txs transmitting to the Rx simultaneously. Consequently, the two signals can reach the Rx synchronously. Moreover, to alleviate the impact of the difference of fading between the two transmission links on reception, we configure the experimental setup to be symmetrical with respect to the bisector AB. This ensures that both signal components undergo similar small-scale fading experience.

The B210 and the X310 devices are synchronized by PC2 controlling the B210 to implement such functions as correlation-based coarse frequency compensation, phase-locked loop (PLL)-based fine frequency compensation, timing recovery with fixed-rate re-sampling, bit stuffing/skipping, and frame synchronization [38]. For simplicity, we equip the Txs and Rx with a single antenna (i.e., $N_{T_0} = N_{T_1} = 1$ and $N_{R_0} = 1$). In this configuration, no spatial precoding or receive filtering is necessary. Consequently, PC1 controls the two Txs to generate and send an interfering BPSK and a recycling BPSK signals, respectively. The main parameters used in the experiment are shown in Table III.

In our experiment, PC1 controls one X310 device, representing AP, to execute BPSK modulation with initial phases $\{\pi/2, 3\pi/2\}$, generating interference s_1 carrying x_1. At the same time, another X310 device, representing the GW, is controlled to perform BPSK modulation with initial phases $\{0, \pi\}$, producing the recycling signal s_{RC} carrying x_{RC}. Since the desired signal can be obtained through the interaction of interference and recycling signal, we can derive the desired data x_0 (the initial phases of QPSK modulation are $\{\pi/4, 3\pi/4, 5\pi/4, 7\pi/4\}$) by adding x_1 and x_{RC}. AP and GW simultaneously transmit their BPSK modulated signals to the IoT device (B210). These two signal components are superimposed at the Rx. The Rx estimates the equivalent CSI between itself and the Txs based on the mixed pilot signals received from AP and GW (we use the Barker code as the pilot sequence), and then compensates the equivalent channel accordingly and adopts the QPSK demodulation module to recover data $\bar{x}_0$ (in

[5]In the experiment, we use a single computer to control the GW and AP for simplicity. This setup is chosen because the objective of this experiment is to demonstrate that the desired signal can be produced through the interaction of interference and a recycling signal. However, it should be noted that this simplification does not restrict the application of our method to scenarios where the devices are not connected to a centralized control center for synchronization. Additionally, with the synchronization schemes such as global positioning system (GPS) and IEEE 1588 precision time protocol (PTP), where GPS can provide nanosecond accuracy and PTP can provide sub-microsecond accuracy [36], both the GW and AP can function as independent devices and can be synchronized at a symbolic level (e.g., the OFDM symbol duration can be tens of microseconds in practice [37]) to enable the use of our scheme.

TABLE III
PARAMETER SETTINGS OF IRC

Carrier frequency	Symbol rate	Interpolation factor	Sampling rate (base-band)	Roll-off factor of raised cosine filter	Transmit gain of each Tx
915MHz	0.2MBaud	2	0.4MHz	0.5	[4dB,15dB]

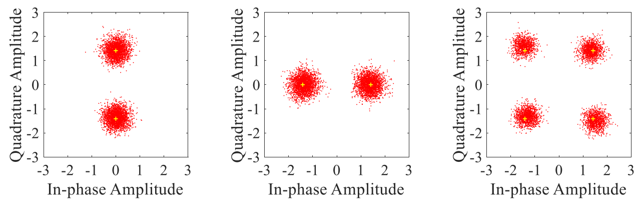

(a) Interference (x_1). (b) IRC signal (x_{RC}). (c) Recycled signal ($\bar{x}_0$).

Fig. 7. Illustration of interference recycling through hardware implementation.

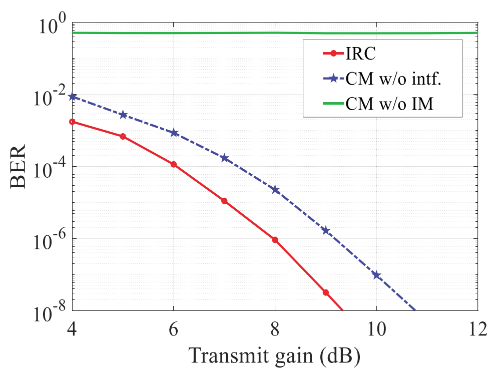

Fig. 8. BER performance of the IoT device.

the demodulation, automatic gain control (AGC) is employed for counteracting path loss and channel attenuation) from the mixed signal.

Fig. 7 illustrates the production of a QPSK symbol $\bar{x}_0$ by combining two BPSK symbols x_1 and x_{RC} at the IoT device. Note that the results shown in Fig. 7 is derived from a hardware experiment. As the figure shows, although the constellations of x_1 and x_{RC} are standard $\frac{\pi}{2}-$BPSK and BPSK constellations, the combined QPSK constellation distorts both in phase and amplitude compared to the standard QPSK constellation. This is because 1) both x_1 and x_{RC} are observed at the Tx-side, without channel attenuation, showing a standard constellation; and 2) while decoding $\bar{x}_0$ from the received mixed signal, we compensate for the channel fading based on the estimation of the equivalent channel of the mixed signal rather than the two individual sub-channels through which the BPSK signals are transmitted. This leads to a residual difference between the propagation of the two signal components. As a result, we observe a distorted QPSK constellation at the Rx.

To corroborate the performance of IRC, we evaluate the bit-error rate (BER) of the IoT device under different assumptions of interference and transmission schemes, as illustrated in Fig. 8. In addition to the proposed IRC, we investigate two other schemes that directly generate and transmit a modulated QPSK signal to its destination. The first scheme — referred to as *centralized modulation (CM) without interference* (w/o intf.) — avoids

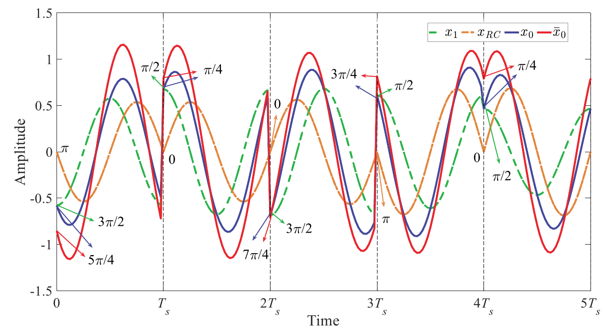

Fig. 9. Waveforms of various data symbols.

interference by shutting off the interferer, while the second scheme — referred to as *CM without IM* — turns on the interferer but lacks interference management. Under CM w/o IM, the GW directly transmits to its serving IoT device under the influence of interference from the AP. As the figure shows, the BER curves of both CM w/o intf. and IRC decrease as the transmit gain rises. With IRC, the interference can be effectively utilized, resulting in a BER superior to that of CM w/o intf. This is because under IRC, two Txs with the same transmit gain are employed, while under CM w/o intf., only one Tx is used. As a result, since IRC can effectively exploit the interference power for desired transmission, it can recover a stronger desired signal than CM w/o intf., lowering BER. With the interference left unmanaged, the IoT device's BER noticeably gets worse. As depicted in the figure, the BER of CM w/o IM is approximately 50%. This is because in our experimental settings, the interference is as strong as the desired signal. Without interference management, the desired transmission can be significantly impaired. Moreover, since the ratio of the transmit gain of the AP to that of the GW is 1 regardless of the variation of transmit gain, the BER of CM w/o IM does not change with an increase of the transmit gain. It is worth noting that in our experiments, both the interferer and the desired Tx employ the same pilot sequence and are well synchronized. Therefore, the interference only affects the decoding of the desired payload. In this scenario, when the interference becomes weak relative to the desired signal, the BER of CM w/o IM may improve. However, in practice, the interference can also disrupt the pilot sequence, thereby affecting the synchronization of the desired signal's reception and resulting in a poor BER.

Fig. 9 plots the waveforms of the interference data x_1, the recycling data x_{RC}, the desired data x_0, and the data decoded from the mixed received signal (denoted as $\bar{x}_0$). For clarity, we only illustrate the amplitudes and phases of 5 symbols in each data sequence. Without loss of generality, we take the first data symbol as an example to demonstrate the validity of IRC. As the figure shows, the phases of x_1, x_0, and x_{RC} are $3\pi/2$, $5\pi/4$, and π, respectively. By decoding the received mixed signal, we can obtain $\bar{x}_0$ with phase $5\pi/4$, which is identical to the phase of x_0. Moreover, as illustrated in Fig. 9, the phase of the decoded

$\bar{x}_0$ is slightly different from that of the desired data x_0. This difference arises due to channel estimation errors. It is important to note, however, that this discrepancy does not compromise the accuracy of IoT device decoding. Additionally, we can see from Fig. 9 that the amplitude of x_0 at the Tx-side is approximately $\sqrt{2}$ times that of x_1 and x_{RC}. This is because x_0 is obtained by superimposing x_1 and x_{RC}, resulting in the power of x_0 being twice that of each component. Furthermore, the amplitude of $\bar{x}_0$ demodulated from the received mixed signal is larger than that of x_0. This is due to the implementation of the automatic gain control (AGC) at the Rx. In our experiment, we set the power coefficient of AGC to be 2. Consequently, we observe that the amplitude of $\bar{x}_0$ is approximately $\sqrt{2}$ times that of x_0. From the aforementioned discussion of the experimental results, we can verify that the proposed IRC can correctly recover the desired data from the mixed received signal, hence effectively utilizing interference.

B. MATLAB Simulation

We now evaluate the performance of the proposed mechanism using MATLAB. Besides IRC proposed in Section IV, and μIRC and OIRC provided in Section V, some typical schemes including IN [7], IS [8], ZF reception, p2pMIMO, and Non-IM are also simulated for the purpose of comparison. Note that IRC, IN, IS, and ZF reception are victim Tx/Rx side while the interfering Tx–Rx pair does not modify its transmission for the victim. Therefore, we investigate the SE of IoT device with various IM schemes. As for ZFBF and IA, since they are interfering Tx-side implementations, IoT device's SE is the same as that of p2pMIMO, i.e., interference to the IoT device is avoided by AP-side pre-processing. Moreover, it is worth noting that as long as the GW transmits to the IoT device, regardless of the recycling signal (with our approach) or the desired signal (with conventional communication methods), the signal from GW will cause interference at the WiFi station. As we focus on designing interference recycling for IoT system while suggesting that the WiFi system continues to use existing conventional methods for IM, in subsequent simulations, we only investigate the performance of IoT device. Regarding the SNR and data rate of the WiFi station, the analysis can be done similarly to that of the IoT device, as given by (23).

We set $N_{T_i} = N_{R_i} = 2^6$ where $i \in \{0, 1\}$. Both the WiFi and IoT transmissions employ BF and BPSK modulation. We define $\bar{\zeta} = 10\lg(P_{T_1}/\sigma_n^2)$ and $\varepsilon = \sqrt{P_{T_1}}/\sqrt{P_{T_0}}$, and adopt $\bar{\zeta} \in [0, 20]$ dB and $\varepsilon \in [0.3, 10]$ in our simulation. Although our evaluation is done with some specific parameter settings, a similar conclusion can be drawn for more general cases. In the following simulation, when IRC, μIRC, OIRC, IN or IS are inapplicable due to insufficient Tx power budget, we simply switch off the corresponding method and adopt Non-IM.

Fig. 10 shows the variation of IoT device's instantaneous SE with μ under $\varepsilon = 0.5$ and $\bar{\zeta} = 10$dB, given an arbitrary

[6]When the number of antennas on an IoT device or GW increases, the reception of the recycling signal at the interfered IoT device is enhanced, facilitating the utilization of interference and thus outputting a stronger desired signal. However, the increase in the number of antennas on a WiFi AP does not necessarily lead to increased interference. This is because the WiFi AP typically targets its serving STA, and as the number of AP antennas increases, the leakage of interference towards the IoT device may actually decrease, thereby limiting the exploitable interference.

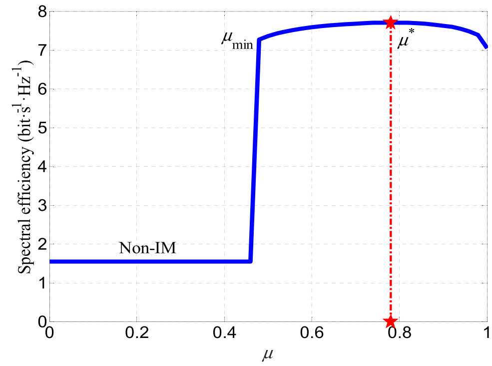

Fig. 10. IoT device's instantaneous SE versus μ with μIRC under $\varepsilon = 0.5$ and $\bar{\zeta} = 10$ dB.

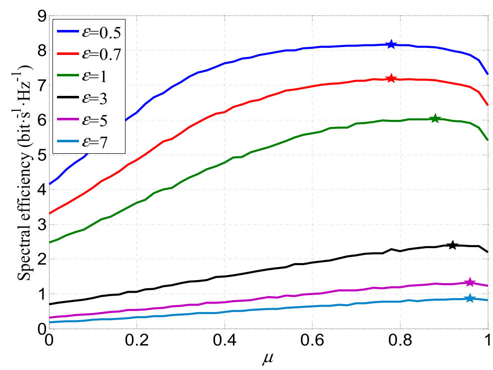

Fig. 11. IoT device's average SE versus μ under $\bar{\zeta} = 10$dB and different ε.

channel realization. As the figure shows, an optimal μ^* computed in terms of (29) exists which can achieve the maximum IoT device's SE. In the figure, $\mu_{\min}$ denotes the minimum power allocation coefficient for implementing interference recycling. When $\mu < \mu_{\min}$, IRC is not applicable due to insufficient transmit power at the GW. In such a case, the IoT transmission-pair simply switches off IRC and employs Non-IM mode. When $1 \geq \mu > \mu_{\min}$, the IoT device's SE increases first and then decreases as μ increases, and reaches the peak at μ^* (marked by pentagram).

Fig. 11 plots the IoT device's average SE along with μ under $\bar{\zeta} = 10$ dB and different ε. As the figure shows, given fixed ε, the IoT device's average SE grows first and then reduces as μ increases. The maximum value of average SE is marked by pentagram, corresponding to the optimal μ^* in a statistical average sense. Given $\bar{\zeta} = 10$ dB, and fixed interference strength, the GW's transmit power reduces with the increase of ε, decreasing IoT device's SE. Moreover, as ε grows, GW's power decreases relative to the interference strength, so GW needs to spend a larger portion of power for interference recycling, making the average optimal μ^* gradually approach 1.

Fig. 12 plots the IoT device's average SE with various IRC designs. As ε increases, P_{T_0} is shown to become smaller than P_{T_1}, decreasing IoT device's SE for all schemes. Since Modes III and I are equivalent in *power efficiency* measured in bps/W, they yield the same SE as analyzed in Section V. Because the realization of Modes II and IV are within the right and left triangle areas of Fig. 4, we simulate the average SE over these two areas. Moreover, as Mode II under-utilizes interference while the other three fully exploit the interference, Mode II outputs

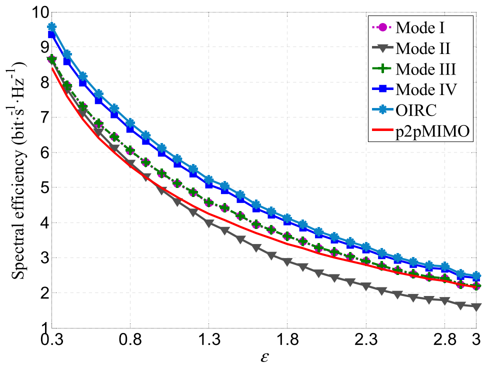

(a) $\bar{\zeta} = 0$dB.

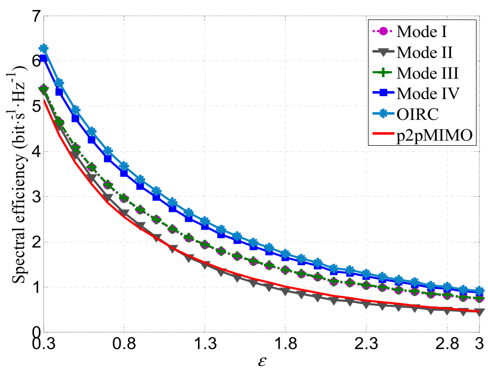

(b) $\bar{\zeta} = 10$dB.

Fig. 12. IoT device's average SE versus ε with various IRC designs for different $\bar{\zeta}$.

the lowest SE, even lower than p2pMIMO (IA, ZFBF) when the interference is strong. As discussed in Section V-A, Mode IV is the most power-efficient of the four modes, and hence we also simulate Mode IV with the optimal transmit power allocation to the direct desired data transmission and recycling signal, i.e., OIRC, which provides the maximum IoT device's SE.

Fig. 13 shows the IoT device's average SE along with $\bar{\zeta}$ of different IRC designs. As one can see from Fig. 13(a), when $\varepsilon = 0.5$, P_{T_0} is strong relative to P_{T_1}, and thus the GW has sufficient power for interference recycling, so the SE of Mode I, III, IV, and OIRC is higher than that of p2pMIMO, while Mode II which is less power-efficient than the other modes, outputs SE close to p2pMIMO (IA, ZFBF). In Fig. 13(b), given $\varepsilon = 2$, interference to the IoT device becomes stronger as $\bar{\zeta}$ grows, then more power is needed at the GW for interference recycling, causing the feasible probability of all IRC realizations to drop. Therefore, various IRC designs yield almost the same or even inferior SE to that of p2pMIMO (IA, ZFBF) at high $\bar{\zeta}$ regime, e.g., when $\bar{\zeta} > 15$dB, SE of p2pMIMO (IA, ZFBF) is close to that of OIRC and Mode IV while outperforming Mode I, II, and III.

Fig. 14 plots the IoT device's average SE along with ε for different IM schemes where $\varepsilon \in [0.3, 3]$. The SE of all schemes is shown to decrease as ε grows, which is consistent with the results in Fig. 14. The proposed IRC (Mode I as illustrated in Fig. 4) outputs the second highest SE of all mechanisms, because such an IRC implementation can make full use of interference. Moreover, since OIRC can optimally utilize the GW's transmit power, its SE performance is improved further than that of IRC. Note that p2pMIMO (IA, ZFBF) is realized by letting the GW transmit to the IoT device in accordance with their own transmission channel $\mathbf{h}_0$ without interference. In such a case, SE of p2pMIMO (IA, ZFBF) is the product of power P_{T_0}. As for the IRC, GW sends a recycling signal with power P_{T_0} and exploits the interference power at the victim IoT device, and thus SE of IRC is the output of power larger than P_{T_0}. Therefore, OIRC and IRC significantly outperform p2pMIMO (IA, ZFBF) in SE. In Fig. 14(a), when $\bar{\zeta}$ is small, the interference is weak relative to noise. In such a case, noise dominates the SE performance, so the contribution of IM to SE is limited, incurring ZF and IN inferior to Non-IM.

Fig. 14(b) shows the case when the interference is stronger than noise ($\bar{\zeta} = 10$ dB). In such a case, IM contributes more to SE enhancement, yielding higher SE than Non-IM, especially for ZF and IS for small ε. Moreover, IS outperforms ZF when $\varepsilon < 1.3$, and the opposite holds given a larger ε. This is because when ε is small, P_{T_0} is strong relative to P_{T_1}, ZF reception incurs more desired signal's power loss while nullifying interference at the IoT device, whereas for IS, only the effective portion of interference on the desired transmission of IoT device is counteracted. As ε grows larger, P_{T_1} becomes strong relative to P_{T_0}, and ZF can thus mitigate more interference with the same desire signal's power loss, whereas for IS, more transmit power at the GW is consumed for generating the steering signal. Hence, ZF outperforms IS as $\varepsilon > 1.3$. Given fixed $\bar{\zeta}$, the interference perceived by the IoT device determined by P_{T_1}, becomes strong relative to P_{T_0} as ε increases, reducing IRC's feasible probability. Therefore, SE of IRC approaches that of p2pMIMO (IA, ZFBF) as ε becomes very large. Since OIRC is optimal among all possible IRC implementations, its SE exceeds that of the other schemes, but the gap is reduced slightly as ε becomes large.

Fig. 15 shows the IoT device's average SE of different IM methods along with $\bar{\zeta}$ where $\bar{\zeta} \in [0, 20]$ dB. Given fixed ε, both P_{T_0} and P_{T_1} increase as $\bar{\zeta}$ grows, thus making more power available at the GW and increasing the SE of all schemes with an increase of $\bar{\zeta}$. Fig. 15(a) shows OIRC (IRC) to provide the best (second best) SE among all the schemes. p2pMIMO (IA, ZFBF) is the third while IS is the fourth. Given a relatively strong interference, i.e., $\bar{\zeta} > 3$dB, ZF outperforms IN and Non-IM, while Non-IM yields the lowest SE. This can be reasoned as in the discussion of Fig. 14. Given $\varepsilon = 0.5$, the GW has sufficient power for desired signal's transmission and interference management such as IS, IN, IRC, and OIRC, thus yielding higher SE than that in Fig. 15(b) under $\varepsilon = 2$. In Fig. 15(b), P_{T_1} is strong relative to P_{T_0}, but, when $\bar{\zeta}$ is small, interference at the IoT device is weak, and hence the feasibility of IRC and OIRC is high enough, yielding better SE than p2pMIMO (IA, ZFBF). As $\bar{\zeta}$ increases further, the feasible probability of IRC and OIRC drops, thus yielding almost the same as or even inferior SE to that of p2pMIMO (IA, ZFBF). However, IRC and OIRC still outperform IS, IN, ZF, and Non-IM.

In summary, the proposed interference recycling schemes, including IRC, μIRC, and OIRC, not only outperform existing interfered/victim-side IM schemes such as ZF, IN, and IS, but also exceed ZFBF and IA which are implemented at the interfering Tx to achieve high SE of the victim transmission-pair (GW and IoT device in this paper) as long as ε or/and $\bar{\zeta}$ are not too large. Moreover, OIRC is the best among all the realizations of interference recycling.

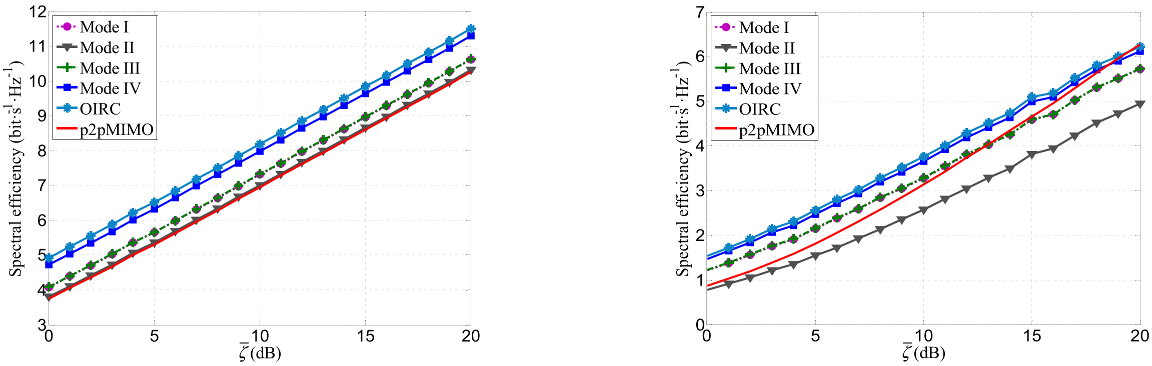

(a) $\varepsilon = 0.5$. (b) $\varepsilon = 2$.

Fig. 13. IoT device's average SE versus $\bar{\zeta}$ with various IRC designs for different ε.

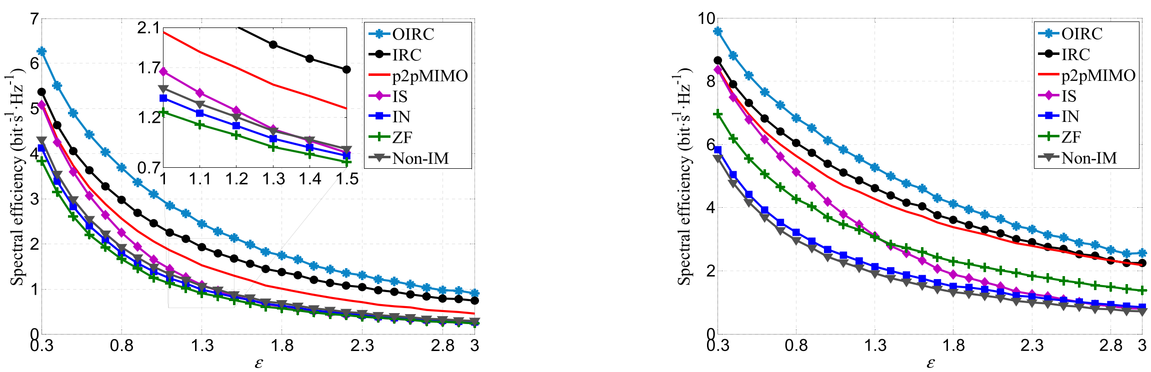

(a) $\bar{\zeta} = 0$dB. (b) $\bar{\zeta} = 10$dB.

Fig. 14. IoT device's average SE versus ε with various IM schemes for different $\bar{\zeta}$.

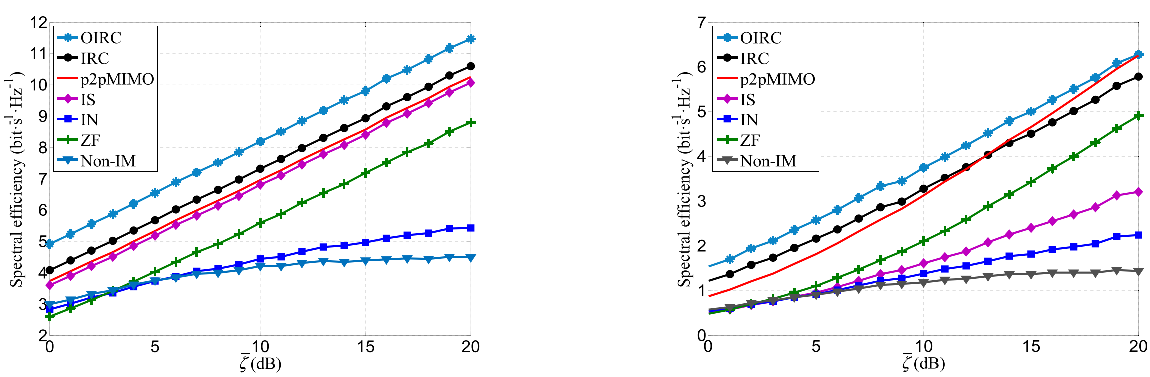

(a) $\varepsilon = 0.5$. (b) $\varepsilon = 2$.

Fig. 15. IoT device's average SE versus $\bar{\zeta}$ with various IM schemes for different ε.

VII. Conclusion

In this paper, we have proposed a new interference management scheme, called *Interference ReCycling* (IRC). By exploiting both CSI and data information carried in the interference, a recycling signal is generated and then sent by the interfered/victim Rx's associated Tx. Using the recycling signal, the desired data of the interfered Tx–Rx pair can be recovered from the interference at the victim Rx. Moreover, by properly distributing the transmit power used for the recycling signal and the desired signal's transmission, the performance of interfered Tx–Rx pair can be improved further. Our theoretical analysis, experimental and numerical evaluations show that the proposed IRC schemes can fully exploit interference, and hence can significantly improve the spectral efficiency of the victim Rx over the other existing methods.

References

[1] L. S. Vailshery, "Number of IoT connected devices worldwide 2019–2023, with forecasts to 2030," 2023. [Online]. Available: https://www.statista.com/statistics/1183457/iot-connected-devices-worldwide/

[2] A. Ö. Ercan, M. O. Sunay, and I. F. Akyildiz, "RF energy harvesting and transfer for spectrum sharing cellular IoT communications in 5G systems," *IEEE Trans. Mobile Comput.*, vol. 17, no. 7, pp. 1680–1694, Jul. 2018.
[3] Ericsson.com, "White paper: Cellular IoT in the 5G era," 2023. [Online]. Available: https://www.ericsson.com/en/reports-and-papers/white-papers/cellular-iot-in-the-5g-era
[4] R. F. Ustok, P. A. Dmochowski, P. J. Smith, and M. Shafi, "Interference cancellation with jointly optimized transceivers in multiuser multicellular networks," *IEEE Trans. Veh. Technol.*, vol. 67, no. 8, pp. 7219–7229, Aug. 2018.
[5] C. M. Yetis, T. Gou, S. A. Jafar, and A. H. Kayran, "On feasibility of interference alignment in MIMO interference networks," *IEEE Trans. Signal Process.*, vol. 58, no. 9, pp. 4771–4782, Sep. 2010.
[6] S. A. Jafar and S. Shamai, "Degrees of freedom region of the MIMO X channel," *IEEE Trans. Inf. Theory*, vol. 54, no. 1, pp. 151–170, Jan. 2008.
[7] H. Zeng, X. Yuan, X. Qin, Y. Shi, Y. T. Hou, and W. Lou, "Nullification in the air: Interference neutralization in multi-hop wireless networks," in *Proc. IEEE Int. Conf. Comput. Commun.*, 2016, pp. 1–9.
[8] Z. Li, T. Liu, K. G. Shin, J. Liu, and Z. Yan, "Interference steering to manage interference in IoT," *IEEE Internet Things J.*, vol. 6, no. 6, pp. 10458–10471, Dec. 2019.
[9] H. Wang and A. O. Fapojuwo, "Design and performance evaluation of successive interference cancellation-based pure aloha for Internet-of-Things networks," *IEEE Internet Things J.*, vol. 6, no. 4, pp. 6578–6592, Aug. 2019.
[10] P. Chen, Z. Xie, Y. Fang, Z. Chen, S. Mumtaz, and J. J. P. C. Rodrigues, "Physical-layer network coding: An efficient technique for wireless communications," *IEEE Netw.*, vol. 34, no. 2, pp. 270–276, Mar./Apr. 2020.
[11] D. Ma, G. Lan, M. Hassan, W. Hu, and S. K. Das, "Sensing, computing, and communications for energy harvesting IoTs: A survey," *IEEE Commun. Surv. Tut.*, vol. 22, no. 2, pp. 1222–1250, Second Quarter 2020.
[12] M. Cansiz, D. Altinel, and G. K. Kurt, "Efficiency in RF energy harvesting systems: A comprehensive review," *Energy*, vol. 174, pp. 292–309, 2019.
[13] Z. Li, J. Chen, K. G. Shin, and J. Liu, "Interference recycling: Exploiting interfering signals to enhance data transmission," in *Proc. IEEE Int. Conf. Comput. Commun.*, 2019, pp. 100–108.
[14] Z. Li, K. G. Shin, and L. Zhen, "When and how much to neutralize interference?," in *Proc. IEEE Int. Conf. Comput. Commun.*, 2017, pp. 1–9.
[15] S. C. Liew, L. Lu, and S. Zhang, *A Primer on Physical-Layer Network Coding*. San Rafael, CA, USA: Morgan & Claypool, 2015.
[16] P. Kamalinejad, C. Mahapatra, Z. Sheng, S. Mirabbasi, V. C. M. Leung, and Y. L. Guan, "Wireless energy harvesting for the Internet of Things," *IEEE Commun. Mag.*, vol. 53, no. 6, pp. 102–108, Jun. 2015.
[17] T. Sanislav et al., "Wireless energy harvesting: Empirical results and practical considerations for Internet of Things," *J. Netw. Comput. Appl.*, vol. 121, pp. 149–158, 2018.
[18] B. Clerckx, Z. Popović, and R. Murch, "Future networks with wireless power transfer and energy harvesting [Scanning the Issue]," *Proc. IEEE*, vol. 110, no. 1, pp. 3–7, Jan. 2022.
[19] Y. Liu, S. A. Mousavifar, Y. Deng, C. Leung, and M. Elkashlan, "Wireless energy harvesting in a cognitive relay network," *IEEE Trans. Wireless Commun.*, vol. 15, no. 4, pp. 2498–2508, Apr. 2016.
[20] W. Rafique, L. Qi, I. Yaqoob, M. Imran, R. U. Rasool, and W. Dou, "Complementing IoT services through software defined networking and edge computing: A comprehensive survey," *IEEE Commun. Surv. Tut.*, vol. 22, no. 3, pp. 1761–1804, Third Quarter 2020.
[21] W. Ren, Y. Sun, H. Luo, and M. Guizani, "A novel control plane optimization strategy for important nodes in SDN-IoT networks," *IEEE Internet Things J.*, vol. 6, no. 2, pp. 3558–3571, Apr. 2019.
[22] Y. Nagai, J. Guo, P. Orlik, T. Sumi, B. A. Rolfe, and H. Mineno, "Sub-1GHz frequency band wireless coexistence for the Internet of Things," *IEEE Access*, vol. 9, pp. 119648–119665, 2021.
[23] B. Kurungadan and A. Abdrabou, "Using software-defined networking for data traffic control in smart cities with WiFi coverage," *Symmetry*, vol. 14, no. 10, pp. 1–17, 2022.
[24] ARUBA, "ARUBA IoT gateway solution," 2023. [Online]. Available: https://www.cwnp.com/uploads/aruba-iot-gateway-solution-a-whitepaper-by-cwne-candidate-(approved)-yannick-schappler.pdf
[25] H. Qin, B. Cao, J. He, X. Xiao, W. Chen, and Y. Peng, "Cross-interface scheduling toward energy-efficient device-to-gateway communications in IoT," *IEEE Internet Things J.*, vol. 7, no. 3, pp. 2247–2262, Mar. 2020.
[26] F. Rincon, Y. Tanaka, and T. Watteyne, "On the impact of WiFi on 2.4 GHz industrial IoT networks," in *Proc. IEEE Int. Conf. Ind. Internet*, 2018, pp. 33–39.
[27] P. Yang, L. Yang, and S. Wang, "Performance analysis for RIS-Aided wireless systems with imperfect CSI," *IEEE Wireless Commun. Lett.*, vol. 11, no. 3, pp. 588–592, Mar. 2022.
[28] V. Jungnickel et al., "Backhaul requirements for inter-site cooperation in heterogeneous LTE-Advanced networks," in *Proc. IEEE Int. Conf. Commun.*, 2013, pp. 905–910.
[29] "Coordinated multi-point operation for LTE physical layer aspects," 3rd General Partnership Project (3GPP), document TR 36.819 R11 V11.2.0, 2013.
[30] L. Schulz, K. Manolakis, and V. Jungnickel, "Adaptive feedback compression for joint transmission coordinated multi-point," in *Proc. IEEE Veh. Technol. Conf.*, 2013, pp. 1–6.
[31] S. Verma, T. K. Rodrigues, Y. Kawamoto, M. M. Fouda, and N. Kato, "A survey on Multi-AP coordination approaches over emerging WLANs: Future directions and open challenges," *IEEE Commun. Surv. Tut.*, vol. 26, no. 2, pp. 858–889, Second Quarter 2024.
[32] L. Zhang, H. Yin, S. Roy, and L. Cao, "Multiaccess point coordination for next-gen Wi-Fi networks aided by deep reinforcement learning," *IEEE Syst. J.*, vol. 17, no. 1, pp. 904–915, Mar. 2023.
[33] K. Yip, Y. Wu, and T. Ng, "Timing-synchronization analysis for IEEE 802.11a wireless LANs in frequency-nonselective rician fading environments," *IEEE Trans. Wireless Commun.*, vol. 3, no. 2, pp. 387–394, Mar. 2004.
[34] G. Miao, N. Himayat, and G. Y. Li, "Energu-efficient link adaptation in frequency-selective channels," *IEEE Trans. Commun.*, vol. 58, no. 2, pp. 545–554, Feb. 2010.
[35] R. Jäntti, R. D. Candia, R. Duan, and K. Ruttik, "Multiantenna quantum backscatter communications," in *Proc. IEEE Globecom Workshops*, 2017, pp. 1–6.
[36] S. Zhu, X. Zheng, L. Liu, and H. Ma, "AirSync: Time synchronization for large-scale IoT networks using aircraft signals," *IEEE Trans. Mobile Comput.*, vol. 22, no. 1, pp. 69–83, Jan. 2023.
[37] Evolved Universal Terrestrial Radio Access (E-UTRA), "Physical channels and modulation," 3rd General Partnership Project (3GPP), document TS 36.211 R18 v18.0.1, 2024.
[38] MathWorks: QPSK Receiver with USRP$^{\mathrm{TM}}$Hardware in Simulink - MATLAB & Simulink Example. 2022. [Online]. Available: https://ww2.mathworks.cn/help/supportpkg/usrpradio/ug/qpsk-receiver-with-usrp-hardware-in-simulink.html?s_tid=srchtitle_USRP%20QPSK_3

Zhao Li (Member, IEEE) received the BS degree in telecommunications engineering, and the MS and PhD degrees in communication and information systems from Xidian University, Xi'an, China, in 2003, 2006, and 2010, respectively. He worked as a visiting scholar and then research scientist with the Real-Time Computing Laboratory, Department of Electrical Engineering and Computer Science, University of Michigan, from 2013 to 2015. He is currently an associate professor with the School of Cyber Engineering, Xidian University. He has published more than 60 technical articles with premium international journals and conferences, such as *IEEE Transactions on Mobile Computing (TMC)*, *IEEE Transactions on Wireless Communications (TWC)*, *IEEE Internet of Things Journal*, IEEE INFOCOM, *IEEE Transactions on Vehicular Technology (TVT)*, *Computer Communications*, and *Wireless Networks*. His research interests include wireless communication, 5G communication systems, resource allocation, interference management, the IoT, and physical layer security.

Lijuan Zhang is currently working toward the master's degree with the School of Cyber Engineering, Xidian University. Her research interests include physical layer security and reconfigurable intelligent surface.

Chengyu Liu is currently working toward the master's degree with the School of Cyber Engineering, Xidian University. His research interests include physical layer security and reconfigurable intelligent surface.

Siwei Le is currently working toward the master's degree with the School of Cyber Engineering, Xidian University. His research interests include physical layer security and network simulation.

Jie Chen, photograph and biography not available at the time of publication.

Kang G. Shin (Life Fellow, IEEE) received the BS degree in electronics engineering from Seoul National University, Seoul, South Korea, in 1970, and the MS and PhD degrees in electrical engineering from Cornell University, Ithaca, New York, in 1976 and 1978, respectively. He is currently the Kevin and Nancy O'Connor professor of computer science and the founding director of the Real-Time Computing Laboratory, Department of Electrical Engineering and Computer Science, University of Michigan, Ann Arbor, Michigan. At Michigan, he has supervised the completion of 82 PhDs and also chaired the Computer Science and Engineering Division for three years starting, in 1991. From 1978 to 1982, he was on the faculty of the Rensselaer Polytechnic Institute, Troy, New York. He has authored/coauthored more than 900 technical articles (more than 330 of which are published in archival journals) and more than 30 patents or invention disclosures. His current research interests include QoS-sensitive computing and networks, as well as on embedded real-time and cyber-physical systems. He is also a fellow of ACM. He received numerous institutional awards and best paper awards.

Zheng Yan (Fellow, IEEE) received the BEng degree in electrical engineering, the MEng degree in computer science and engineering from Xi'an Jiaotong University, Xi'an, China, in 1994 and 1997, respectively, the MEng degree in information security from the National University of Singapore, Singapore, in 2000, and the LicSc degree and DSc (Tech.) degree in electrical engineering from the Helsinki University of Technology, Helsinki, Finland, in 2005 and 2007, respectively. She is currently a distinguished professor with Xidian University. She has published over 400 papers in prestigious journals and conferences worldwide, including IEEE Security and Privacy, IEEE Transactions on Information Forensics and Security, IEEE Transactions on Dependable and Secure Computing, IEEE INFOCOM, and ACM/ICCC ICSE. She is the inventor and the co-inventor of more than 110 patents and 50 PCT patent applications. Her research interests include trust, security and privacy, social networking, cloud computing, networking systems, and data mining. She also serves as an Executive Editor-in-Chief of *Information Sciences* and Area Editor/Associate Editor/Editorial Board Member of over 60 journals, including *ACM Computing Surveys, Information Fusion, IEEE Internet of Things Journal, IEEE Network Magazine*, etc. She has served as a General Chair or Program Committee Chair for over 40 international conferences and has delivered over 30 keynote and invited talks at international conferences and renowned enterprises.

Jia Liu (Senior Member, IEEE) received the BE degree from the School of Telecommunications Engineering, Xidian University, Xi'an, China, in 2010, and the PhD degree from the School of Systems Information Science, Future University Hakodate, Hakodate, Japan, in 2016. He has published more than 60 academic papers with premium international journals and conferences, such as *IEEE Transactions on Wireless Communications (TWC)*, *IEEE Transactions on Information Forensics and Security*, and IEEE INFOCOM. His research interests include wireless systems security, space-air-ground integrated networks, Internet of Things, 6G, etc. He received the 2016 and 2020 IEEE Sapporo Section Encouragement Award.